Title
Spin Determination and Physics Beyond the Standard Model at the LHC and ILC

Author
Rentala, Vikram

Publication Date
2010

Peer reviewed|Thesis/dissertation

Spin Determination and Physics Beyond the Standard Model at the LHC and ILC

by

Vikram Rentala

A dissertation submitted in partial satisfaction of the

requirements for the degree of

Doctor of Philosophy

in

Physics

in the

Graduate Division

of the

University of California, Berkeley

Committee in charge:

Hitoshi Murayama, Chair

Christian Bauer

Alexei V. Filippenko

Spring 2010

Spin Determination and Physics Beyond the Standard Model at the LHC and ILC

Abstract

Spin Determination and Physics Beyond the Standard Model at the LHC and ILC

by

Vikram Rentala

Doctor of Philosophy in Physics

University of California, Berkeley

Hitoshi Murayama, Chair

Many of the proposed solutions to the hierarchy and naturalness problems postulate new "partner" fields to the Standard Model (SM) particles. Determining the spins of these new particles will be critical in distinguishing among the various possible SM extensions, yet proposed methods rely on the underlying models. We propose a new model-independent method for spin measurements which takes advantage of quantum interference among helicity states. By looking at the azimuthal angular dependence of the differential cross section in the production followed by decay of a new particle species one can determine its spin by looking at the various cosine modes. We demonstrate that this method will be able to discriminate scalar particles from higher spin states at the ILC, and discuss application to higher spins and possible uses at the LHC. Supersymmetry and Universal Extra Dimensions models prove problematic at the LHC because missing energy signatures result in too many unknowns while reconstructing events. However, warped extra dimension models in certain setups allow for events whose kinematics can be fully reconstructed. In such scenarios, the heavy spin-2 Kaluza-Klein (KK) graviton provides a unique signature with a $\cos(4\phi)$ mode.We study the feasibility of this approach to measuring the spin of the KK graviton in the warped Randall-Sundrum Model at the LHC.

In chapter 5 of this thesis, taking a phenomenological approach, we study a color sextet scalar at the LHC. We focus on the QCD production of a color sextet pair $\Phi_6\bar{\Phi}_6$ through gg fusion and $q\bar{q}$ annihilation. Its unique coupling to $\bar{\psi}^c\psi$ allows the color sextet scalar to decay into same-sign diquark states, such as $\Phi_6 \to tt/tt^*$. We propose a new reconstruction in the multijet plus same sign dilepton with missing transverse energy samples ($bb + \ell^\pm\ell^\pm + \not{E}_T + Nj$, $N \geq 6$) to search for on-shell $tt\bar{t}\bar{t}$ final states from sextet scalar pair production. Thanks to the large QCD production, the search covers the sextet mass range up to 1 TeV for 100 fb^{-1} integrated luminosity.

Koteshwar Rao had been the biggest influence in my love for physics and mathematics. He instilled in me a strong sense of scientific integrity and belief in the scientific method. His insistence on questioning everything and not trusting “authorities” has been a guiding principle in my life. R.I.P.

Contents

List of Figures

List of Tables

Acknowledgments

I want to thank my advisor Hitoshi Murayama. His patience in explaining many physical concepts and the depth of insight that he provided have been invaluable to me. He has been an exceptional personal mentor as well, investing a great deal of time in overseeing not just my development as a physicist but my personal well-being too. I would like to thank the excellent teachers from my high school, IIT Bombay, and UC Berkeley. In particular, I would like to thank my undergraduate thesis advisor S. Umasankar. Among my high school teachers, I would like to especially thank C. Ramaiah and Koteshwar Rao.

The exceptional staff at Berkeley and IPMU have been supremely helpful in everything. A big thanks to the grad students at the BCTP and at TASI 2009 for providing many memorable moments. I would like to thank my fiancé, Nirupama Kulkarni for being understanding of my year and a half long excursion to Japan. I thank my parents and my sister for their love and support over the years.

Part I

First Part

Chapter 1

Introduction

1.1 The Standard Model

The Standard Model (SM) of particle physics is described by an $SU(3)_c \otimes SU(2)_L \otimes U(1)_Y$ gauge theory. Here, the $SU(3)_c$ represents strong interactions of "colored" particles (Quantum Chromodynamics or QCD), responsible for holding together protons and neutrons in the nuclei of atoms and $SU(2)_L \otimes U(1)_Y$ represents the electroweak interaction which spontaneously breaks down to a theory of electromagnetism and is also responsible for nuclear β-decay.

The particle content of the SM is as follows. Fermions in the SM are all spin-$1/2$ and are split into two categories, quarks and leptons. Quarks are charged under $SU(3)_c$ and are said to be colored. There are 3 left-handed quark electroweak or $SU(2)_L$ doublets, each of which comes in 3 colors. There are three left-handed lepton doublets. Additionally, there are 6 right-handed quark singlets (again in three colors each) and 3 right-handed lepton singlets.

Bosons in the SM are of two types, the vector gauge bosons of spin-1 and the Higgs field of spin-0. The gauge bosons are in the adjoint representation of their corresponding gauge groups and hence there are 8 gluon fields, 3 W bosons of $SU(2)_L$, and a B boson field from $U(1)$ hypercharge. The Higgs field acquires a vacuum expectation value (vev) of 250 GeV which is known as the scale of electroweak symmetry breaking (EWSB). This process breaks the $SU(2) \otimes U(1)$ symmetry down to $U(1)_{EM}$, the well-known gauge group of electromagnetism. In this process, the gauge bosons W^+ and W^- (which are linear combinations of the W fields) acquire a mass, along with the Z boson which is a linear combination of the W^3 and B fields. This leaves behind 1 massless gauge boson, which is the photon of electricity and magnetism. In addition to giving mass to the $W^\pm$ and Z gauge bosons, the Higgs field is also believed to generate fermion masses via coupling of left- and right-handed quark and lepton fields. Since the Higgs field is a complex doublet with four real components and three of those components are "eaten" by the gauge bosons when they acquire a mass, this leaves behind a single scalar field called the Higgs field associated with which is the Higgs boson. This is the only particle of the SM that has been predicted but not yet been observed.

The SM of particle physics has been very successful at describing all known particle interactions except gravity. In an effective Quantum Field Theory approach we can include gravitational interactions which are mediated by a massless graviton. However, this theory is non-renormalizable and we expect it to break down at the Planck scale, $\sim 10^{19}$ GeV. There are, however, many unanswered puzzles even within the SM and the framework of TeV-scale physics. In what follows, I will discuss two

significant problems with the SM, one theoretical and the other experimental.

1.2 Problems with the Standard Model

1.2.1 The Hierarchy Problem

The Hierarchy Problem has arguably been one of the driving forces in particle physics model building over the last 30 years. In Quantum Field Theory, the physical masses of particles are determined by a "bare" mass term, which is a parameter in the Lagrangian, added to quantum corrections arising from loop diagrams. Gauge bosons are protected by gauge symmetry and do not acquire a mass unless there is spontaneous symmetry breaking. In the case for fermions, the quantum corrections to the "bare mass" are of the form $m_f \log(\Lambda/m_f)$, where Λ is the cutoff of the theory. It is easy to see that since the correction runs logarithmically with the cutoff, the corrections are small even for a cutoff many orders of magnitude above the scale of the fermion mass. This implies that the theory is valid up to a very high scale (like the Planck scale of $\sim 10^{19}$ GeV). Thus, for fermions, there is no problem in claiming that the theory makes sensible predictions up to very high energies.

The unfortunate problem in the SM, then, appears to be the existence of the scalar field Higgs boson. For a scalar boson, the relationship between the physical mass and the bare mass is given by

$$m_{phys}^2 = m_{bare}^2 - \frac{N_c|y_t|^2}{8\pi^2}\left[\Lambda^2 - 3m_t^2 \log\left(\frac{\Lambda^2 + m_t^2}{m_t^2}\right)\right]. \tag{1.1}$$

Here, only the leading contribution from the diagram with the top quark running in the loop is taken into account. $N_c = 3$ is the number of colors, $y_t \approx 1$ is the top quark Yukawa coupling, and m_t is the top quark mass. The problem is the large quadratic dependence of the quantum correction to the Higgs mass square on the cutoff of the theory.

Since we expect the physical mass of the Higgs to be ~ 100 GeV, we have two choices. First we can take the bare mass to be of the order of the physical mass, and then give up on perturbation theory once our cutoff approaches a few TeV and the correction term becomes comparable to the bare parameter. Alternatively, we can claim a very high cutoff to the theory (say Planck scale, $\sim 10^{19}$ GeV), if we crank up the bare mass in order to give a fine cancelation between the bare mass term and the quantum corrections; this cancelation would have to be very precise, up to one part in 10^{34}. This hierarchy of scales between the electroweak and the Planck scale and the problem of naturalness or "fine tuning" of the bare mass parameter is referred to as the Hierarchy or Naturalness problem. Thus, there is a strong expectation that even if we do find a Higgs boson, we must find new physics at the TeV scale that solves this hierarchy problem.

1.2.2 Dark Matter

Dark matter is matter that pervades the universe but has extremely suppressed or no coupling to electromagnetic waves. The presence of dark matter has thus been inferred through its gravitational coupling in many astrophysical processes such as galactic rotation curves, weak lensing experiments and observations of the cosmic microwave background (CMB). In fact, dark matter is more ubiquitous in the universe than ordinary baryonic matter that we are familiar with. Dark matter makes up about 23 percent of the current energy budget of the universe, whereas baryonic matter makes up only 4 percent

(the rest is dark energy). We would like to measure other interactions of dark matter, if they exist in order to explain the production of dark matter in the early universe. Currently, direct detection experiments have not seen any evidence from dark matter recoiling against nuclei, but have placed strong bounds on such processes. Many models of dark matter parameter space are expected to be tested in the near future. Dark matter provides a strong experimental confirmation that there exists physics beyond the SM that is yet to be understood.

Another fascinating aspect of dark matter is the so-called "WIMP miracle." To get the right abundance of thermally produced dark matter, a weakly interacting massive particle (WIMP), a particle with about TeV-scale mass and weak-scale interaction strength, seems to do the job. This is another indicator that the TeV scale holds interesting physics.

1.3 Solutions to the Hierarchy Problem and Dark Matter candidates

1.3.1 Supersymmetry

Supersymmetry (SUSY) is a symmetry of the Lagrangian that relates bosons (integer spin) and fermions (half-integer spin). If nature were truly supersymmetric this would imply that the electron (say) in the SM would have a spin-0 boson "sfermion" partner (called the selectron) that had exactly the same mass and charge as the electron but differed only in spin. We have not observed any such partners with masses identical to SM particles. Thus, one would expect that if SUSY is a true symmetry of nature, it must be a broken symmetry. The breaking is such that the superpartners to the SM particles have masses larger than their SM counterparts, and from direct search bounds they must be at least a few 100 GeV.

How does SUSY solve the hierarchy problem? SUSY predicts a partner to the top quark called the "stop." The stop also runs in the loop that gives quantum corrections to the Higgs boson mass and by the symmetries of unbroken SUSY gives an equal and opposite contribution to the top loop. If the stop and top mass were identical, as in unbroken SUSY, this would result in an exact cancelation of the quadratic and logarithmic cutoff dependences, thus negating the fine-tuning problem. However, if SUSY is softly broken, this would still lead to a cancelation of the quadratic piece but leave behind a less problematic logarithmic dependence on the cutoff.

In order to not violate the well constrained proton decay limit, one needs to impose a symmetry called R-parity which effectively assigns superpartners a parity of -1 and SM particles a parity of +1. One can easily write down SUSY interactions analogous to SM interactions by taking any SM vertex and replacing two of the incoming lines with superpartners. One interesting consequence of imposing the R-parity symmetry is that the lightest superpartner (LSP) is stable against decay and becomes a viable dark matter candidate.

For a review of SUSY phenomenology, see [4].

1.3.2 Extra Dimensions

Extra dimension theories predict the existence of extra spatial dimensions. Since, these extra dimensions are not visible to us, there are two possibilities. The first is that SM particles cannot propagate in these extra dimensions. That is, all known particles and fields are confined to a 3+1 dimensional "brane." However, since gravity describes the structure of space-time, gravitons or gravity waves can travel in the extra dimensions. The second possibility is that these dimensions are compact or curled up

such that they are too tiny to be readily detectable. It turns out from tests of gravity at small length scales that gravity-only extra dimensions must be sub-millimeter size or less (for flat extra dimensions).

Quantum mechanics predicts an interesting result if extra dimensions are compact. For every known particle that can propagate in the extra dimensions, the momentum in the extra dimension must be quantized in order for the wave function of the particle to be single valued ((anti-)periodic boundary conditions). If p_x is the magnitude of momentum in the extra dimension, it will be of the form n/R for integers n where R is the radius of an extra dimension compactified on a circle S^1. Heuristically, we then have

$$\begin{aligned} E^2 &= m^2 + p'^2 && (1.2)\\ &= m^2 + p^2 + p_x^2 && (1.3)\\ &= \left(m^2 + \frac{n}{R}^2\right) + p^2 && (1.4)\\ &= m_n^2 + p^2. && (1.5) \end{aligned}$$

Here p' is the total magnitude of momentum and p is the magnitude of momentum in the 3 visible spatial dimensions; we have set $c = 1$. Thus, the effect of compact extra dimensions and quantization of momentum in the extra dimension can be treated as an effective set of new particles with masses $m_n^2 = m^2 + (n/R)^2$. So, extra dimensional theories predict a tower of particles, identical to the SM ones but much heavier, with masses $\sim 1/R$ heavier than their SM counterparts. These heavy partners are called Kaluza-Klein (KK) partners. Note that these partners not only have similar charges to their SM counterparts, but they also have excactly the same spins.

Imposing a discrete Z_2 orbifold symmetry on S^1 allows for chiral, zero-mode fermions and prevents proton decay. This symmetry is also known as KK parity. Interestingly, the lightest Kaluza-Klein partner (LKP) is stable against decays in this case and thus gives rise to a viable dark matter candidate.

Just like with SUSY, one can construct vertices by analogy with the SM, by replacing two legs at each vertex with KK partners in such a way that the momentum flow in the extra dimension is conserved and KK parity is respected.

In this thesis we will study only two particular setups for extra dimensions, Universal extra dimensions and Warped Randall-Sundrum (RS) extra dimensions. For a review on the various extra dimension models and phenomenology, see [5].

Universal Extra Dimensions

In this approach, all SM fields propagate in the $d + (3 + 1)$ dimensional bulk where d is the number of extra spatial dimensions. Universal extra dimensions (UED) must be very small, with inverse radii $R^{-1} \sim 300$ GeV in order to satisfy experimental bounds. UED provides a solution to the Hierarchy problem by providing a cutoff at the scale of compactification, which we take to be around a TeV.

Warped Extra Dimensions

Here we describe the so called RS-1 setup. The extra dimension has two branes called the TeV brane and the Planck brane. We will assume for the purposes of this thesis, that only gravity propagates in the 5-d bulk, while the SM fields are confined to a TeV brane. The 5-d bulk has a bulk cosmological

constant, Λ. The two branes have tensions, which are related to the bulk cosmological constant. This setup results in a 5-d metric that has the form

$$ds^2 = e^{-2kr_c\phi}\eta_{\mu\nu}dx^\mu dx^\mu + r_c^2 d\phi^2, \tag{1.6}$$

where k is given in terms of Λ and the 5-d Planck scale. The parameter r_c parameterizes the distance between the two branes. Since the metric has a warped exponential form, we can generate a huge hierarchy between energy scales on the Planck brane and energy scales on the TeV brane by choosing $kr_c \approx 20$ and hence we can solve the hierarchy problem. Note that there is no discrete symmetry in this case and thus we have no natural dark matter candidate. This will, however, turn out to be useful when we do collider studies, since there will be no missing energy signatures. Since in our setup only gravity propagates in the bulk, only gravitons will have KK modes which have a very characteristic spin-2 behavior.

1.4 Distinguishing New Physics by Spin

We have seen that generically, beyond SM (BSM) models predict new particles with identical properties to their SM counterparts; that are heavier but otherwise have similar properties (like couplings) as their SM counterparts. It becomes critical to ask if there is any way we can distinguish between BSM models. One clear distinction between SUSY and extra dimensions theories, such as UED, is that SUSY predicts only one partner per SM particle, whereas UED predicts a whole tower of partners. However, in practise, it is very likely that the energy reach of the LHC may prevent us from accessing the second KK modes. There is, however, one crucial difference that we can still exploit to distinguish between these theories: SUSY predicts partners that are offset by spin-1/2 from their SM counterparts, whereas UED predicts partners with identical spin to their SM counterparts. So, spin measurement of new particles can provide a key tool in distinguishing between models of new physics.

1.5 LHC, ILC, and TeV-scale Physics

The Large Hadron Collider (LHC) is a high energy proton-proton collider. It has been designed to run at 14 TeV center-of-mass energy. Since the partons within the proton carry only a fraction of the proton energy, we expect center-of-mass collisions of the partons to be on the order of a TeV. Thus, the LHC is the first machine that will be able to directly probe the electroweak scale in a controlled setting. The International Linear Collider (ILC) is a proposed linear electron-positron collider that is also expected to probe the electroweak scale. If the LHC discovers new physics at the TeV scale, it will be very hard to pin down precise properties of the new particles because of numerous unknowns, such as the center-of-mass frame for each event. To study precise properties of the new particles, we will need to build a linear collider where we have control over the center-of-mass energy and momentum.

The goals of studying TeV physics have already been established: we expect to find the Higgs boson if it exists, or at least probe the origin of electroweak symmetry breaking. In addition, we expect to find new models of particle physics such as SUSY or UED. Finally, we may also be able to produce dark matter in a lab and study its properties.

1.6 Color Exotics

One aspect of the LHC that is underemphasized is that the LHC is really a QCD machine. New strongly interacting particles such as color sextets and color octets are thus expected to be produced in copious amounts if they exist. These particles are predicted to exist from partial unification theories such as Pati-Salam models [69]. In terms of SU(3) group representations, $3 \otimes 3 = 6 + \bar{3}$. This implies that the color sextet couples to same-sign quarks. Thus, if we produce a heavy color sextet and it decays to two same-sign top quarks, we can pick this signal out easily from the decay of the top quarks into same-sign dileptons. The striking "same sign dilepton" signature of color sextet decay makes it one of the easiest exotic particles to observe at the LHC.

1.7 Organization of This Thesis

This thesis is based on three papers by the author and various collaborators. In chapter 2, we review the problem of spin determination and briefly discuss some proposed techniques to measure spin. In chapter 3, we describe a new model independent spin-determination technique using azimuthal angular dependence. This chapter is based on the work in [1]. The idea will be to produce one or more new particles whose spin we wish to measure and to look at the kinematic distribution of their decay products. The main obstacle to spin determination turns out to be the missing energy signatures that accompany SUSY and UED cascade decays from the stability of the LSP or LKP. We then describe the process of distinguishing between SUSY and UED at a linear collider (where we have control over the center-of-mass energy and momentum). Even at a linear collider, we find that there is a discrete two-fold ambiguity in solving the kinematics of simple decay chains. Applying this to the LHC, where we have no control over the parton energies and hence more unknowns, makes spin measurement at the LHC using this technique a seemingly intractable problem. Thus, in chapter 3 we will only study discrimination between SUSY and UED scenarios at the ILC. In chapter 4, we describe a case where we can solve for the kinematics at the LHC, the case of KK gravitons from RS models. This chapter follows work studied in [2]. In chapter 5, we discuss an entirely new candidate for BSM physics, the color sextet. We analyze the feasibility of detection and measurement of the properties of this new particle. This work is based on [3]. Conclusions to each avenue of inquiry are presented separately within the relevant chapter rather than at the end, to allow for more streamlined reading. We summarize all of our conclusions in a brief note at the end.

Chapter 2

Spin Measurement Techniques

The Large Hadron Collider (LHC) is already up and running, granting us at long last access to the scale of electroweak symmetry breaking and beyond. One of the major puzzles to which we hope the LHC may provide answers is the hierarchy problem [6][7][8][9]: the origin and stability of the orders of magnitude gulf between the Higgs vev at ~ 300 GeV and the Planck scale at $\sim 10^{19}$ GeV. Without experimental results, theorists over the years have collected an impressive array of possible solutions to this problem. Arguably, the leading contender is supersymmetry [10], but there are many others: extra dimensions [11][12][13][14][15][16][17], technicolor [18][7][8], and little Higgs [19] to name a few. Many of these models also provide a long-lived, weakly coupled particle suitable to be a dark matter candidate.

In many of these possibilities the immediate experimental signature from the LHC would be the presence of beyond the SM (SM) particles partnered with some or all of the known particles. For example, the minimal supersymmetric SM (MSSM) doubles the number of particles by adding a new field with the same gauge quantum numbers and Yukawa couplings as in the SM, but spins differing by one half of a unit. Alternatively, the minimal universal extra dimensions (UED) model [20] has compactified extra dimensions which solve the hierarchy problem by 'ending physics' at the scale of electroweak symmetry breaking. That is, the Planck scale of the true $4 + d$ dimensional theory is not far above a TeV, but appears much larger in 4D once the compactification occurs. This results in a tower of KK states, each containing a heavier version of the SM particles with identical quantum numbers, including spin.

It is well known that, due to the similarities in the particle spectrum and quantum numbers, it may be difficult to distinguish the signatures of MSSM particles from the KK=1 modes of UED at future collider experiments [21][22]. The existence of the KK=2 modes could serve as a discriminator between supersymmetry and extra dimensions, but their high masses may make them kinematically inaccessible. Even if produced, they typically decay through KK=1 states, and so their presence would only be felt through an increase in the KK=1 production cross section [23][24]. Determining the spin of the new particles will be necessary to confirm the theory underlying any new particles.

There have been several proposals for measuring spin in future collider experiments. The possibilities at a linear collider are far more numerous, due to the control over the center-of-mass energy in each event. Threshold scans can distinguish scalars from spinors or vector bosons, as the former cross section rises like β^3 while the latter two are proportional to β [25]. However, such a method cannot be used at a hadron collider, and cannot discriminate between spin 1/2 and spin 1. The differential cross

section with respect to production angle in s-channel pair-produced scalars is proportional to $\sin^2\theta$, while for spinors it is $1 + \frac{E^2-m^2}{E^2+m^2}\cos^2\theta$. Model dependence may be present in the form of t-channel diagrams, which introduce a forward peak that is similar for both spin statistics [25]. Such diagrams make the production angle measurement of spin more difficult, but may be possible in some cases [26].

The polar angular dependence in decays can also be used for spin measurements. However, extracting spin from these measurements assumes knowledge of the final state spins and also requires chiral couplings, introducing a model dependence on the spin measurement [27]. While this method was originally proposed for the ILC, it was shown that, with sufficiently long decay chains and exploitation of the asymmetry in production of squarks versus antisquarks, supersymmetric spinors could be distinguished from phase-space decays at the LHC [23][27][28][29][30][31]. Yet this method relies heavily on the underlying models as the entire decay chain must be considered.

Chapter 3

Spin Determination using Azimuthal Angle Dependence at the ILC

Clearly, determination of spin is a problem still requiring novel solutions. In this chapter we investigate a model-independent method to determine the spin of new particles at the ILC, first proposed in [32]. Through interference between the different helicity states in a coherent sum, the cross section of pair-produced particles decaying to two-body final states develops a nontrivial dependence on the azimuthal angle ϕ of the decay. By extracting this dependence, one can determine which helicity states entered into the sum, and thus the spin of the decaying particle. This method is similar to (and was inspired by) the determination of the quark spin measurement at SPEAR [33]. At the end of this chapter, we will discuss how this general method may be extended to the LHC.

This chapter is organized as follows. In section 3.1 we derive the angular dependence of the cross section as a function of particle spin. We then determine appropriate experimental quantities and develop the necessary measurement techniques. In section 3.2 we apply our method to distinguish scalars in pair production at the ILC from production of higher spin states. Spin 1/2 and 1 measurements are considered in section 3.3 and we conclude in section 3.4. Additional calculations are supplied at the end of the chapter in sections 3.5 and 3.6.

3.1 Azimuthal Angular Dependence

To determine the azimuthal dependence of the cross section for pair production followed by decay, we start with a particle of helicity h moving in the $\hat{z}$ direction. When this decays into a two-body final state, the momenta of the daughter particles are confined to a decay plane. If we consider the rotation of this plane about the $\hat{z}$ axis by an angle ϕ, it is clear that the action of the rotation on the matrix element of the decay must be equivalent to the action of the rotation on the parent particle.

Rotations of the particle about the $\hat{z}$ axis introduce a phase $e^{-iJ_z\phi}$, where J_z is the total angular momentum in the $\hat{z}$ direction. However, as the momentum is defined to be in the $\hat{z}$ direction, the orbital component is zero, and J_z reduces to h:

$$J_z = \frac{(\vec{s} + \vec{x} \times \vec{p}) \cdot \vec{p}}{|\vec{p}|} = \frac{\vec{s} \cdot \vec{p}}{|\vec{p}|} = h. \tag{3.1}$$

Therefore, the dependence of the decay matrix element $\mathcal{M}_{decay}$ on ϕ must be

$$\mathcal{M}_{decay}(h,\phi) = e^{ih\phi}\mathcal{M}_{decay}(h,\phi=0). \tag{3.2}$$

Were we to produce particles in only one helicity state, then the total cross section (proportional to the square of $\mathcal{M}_{prod.}\mathcal{M}_{decay}$) would be independent of ϕ. However, if several helicity states are produced and then decay, the total cross section is proportional to the coherent sum squared:

$$\sigma \propto \left| \sum_h \mathcal{M}_{prod.}(h) e^{ih\phi} \mathcal{M}_{decay}(h,\phi=0) \right|^2 . \tag{3.3}$$

This expression is true only within the validity of the narrow-width approximation. However, for 'weakly-coupled' physics, such an approximation is justified [36].

As a result of this interference among the various helicity states, the cross section develops a $\cos(n\phi)$ dependence, where n is an integer running from zero to twice the largest value of h for the decaying particle. That is to say, the ϕ dependences for a scalar, spinor, and massive vector boson can be written as

$$\sigma(s=0) = A_0 \tag{3.4}$$
$$\sigma(s=1/2) = A_0 + A_1\cos(\phi) \tag{3.5}$$
$$\sigma(s=1) = A_0 + A_1\cos(\phi) + A_2\cos(2\phi) \tag{3.6}$$

where the A_i are not functions of ϕ (though they are nontrivial functions of the other kinematics of the problem). The exact forms of the cross section must be worked out from the standard rules of constructing matrix elements from Feynman diagrams, in which case the ϕ dependence will become apparent. However, from this general argument the relationship between spin and ϕ dependence is made clear.

To exploit this ϕ dependence, we consider pair production of particles from e^+e^- at the future ILC. As motivated by solutions to the dark matter problem, we expect the production of particles beyond the SM to cascade down to some weakly coupled particle which will escape the detector. Such WIMPs are present in the supersymmetric spectrum as the lightest supersymmetric particle (LSP), typically the lightest neutralino, or in universal extra dimensions as the lightest Kaluza-Klein odd particle (LKP), typically the B_1. Examples of such event topologies in the UED and SUSY models are shown in Fig. 3.1. However, our methods do not rely on such specific models.

Measuring the azimuthal dependence of the cross section requires that we are able to reconstruct the momentum of the parent particle. For simplicity, we specialize to cases where the pair-produced particles each decay to a charged lepton and missing energy, in which case the events of interest consist of $\ell^{\pm}\ell^{\mp}\not{E}$. While we risk losing some model independence at this stage, such signatures are fairly generic in many extensions to the SM.

Let the pair-produced particles whose spin we wish to measure (μ_1 in Fig. 3.1a or $\tilde{\mu}$ in Fig. 3.1b) have 4-momenta p_A and p_B and mass M . These particles each decay to visible (effectively massless) leptons and a weakly coupled particle with mass m (the $\tilde{\chi}_1^0$ or B_1 in Fig. 3.1). We label the visible lepton momentum p_1 and p_2, and assume that the particles running in each leg are identical. The production angle θ and decay angles θ_i and ϕ_i ($i=1$ for the decay of A and $i=2$ for the decay of B) defined relative to the production plane are shown in Fig. 3.2.

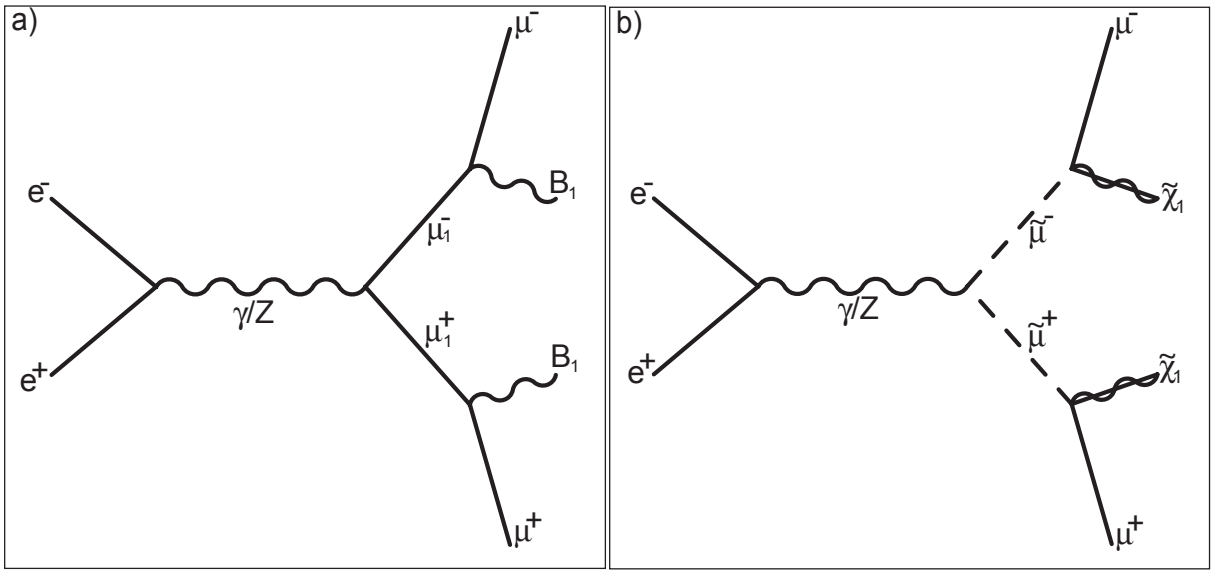

Figure 3.1: a) Pair production of KK$=1$ muons in universal extra dimensions decaying to opposite-sign muons and missing energy in the form of two B_1 gauge bosons (the LKP). b) Pair production of smuons in supersymmetry decaying to opposite-sign muons and the lightest neutralinos as LSP missing energy

At the ILC, assuming knowledge of the masses M and m, it is possible to completely reconstruct the 4-momenta p_A and p_B (and thus the angles ϕ_1 and ϕ_2) up to a two-fold ambiguity [37][38]. We note that there are 4 unknown values for both of the missing particles in the decay, for a total of 8 unknowns. There are 4 measured values of the total missing 4-momentum $\not{p}$; also, for each massive particle in the diagram there is a mass relation, for a total of 4 constraints. Therefore, one would expect this event to be completely reconstructible. When solving the mass relations, however, one finds an ambiguity in sign when taking a square root, leading to the two-fold ambiguity in the reconstructed momentum. For the details of the reconstruction, see Appendix 3.5.

With less than perfect knowledge of the masses, muon momenta, and center-of-mass energy (from beamstrahlung [39] and initial state radiation), the true solution will not be reconstructed perfectly. At the ILC, the masses of lepton and gaugino partners are expected to be measured to one part per mille [40][41], the tracking resolution as good as $\sim 5 \times 10^{-5}(p_T/\text{GeV})$ [42], and beamstrahlung/ISR should be a few percent [43]. Thus, we expect that the errors introduced in ϕ from these effects will be minimal.

As we have two solutions for the momenta p_A and p_B, this leads to two solutions each for ϕ_1 and ϕ_2. The extracted signal in the azimuthal distribution is therefore obtained in the combination of the true and false solutions and compared to the expected values given in Eqs. (3.4), (3.5), and (3.6). In particular, a particle of spin $n/2$ should have $A_i = 0$ for all $i > n$.

3.2 Scalars vs. Spinors

To demonstrate the utility of this method of spin determination, we consider the pair production of scalar right-handed smuons in supersymmetry which decay to muons and LSP $\tilde{\chi}_1^0$s ($e^-e^+ \to \tilde{\mu}_R^-\tilde{\mu}_R^+ \to \mu^-\mu^+\tilde{\chi}_1^0\tilde{\chi}_1^0$). We compare the azimuthal distributions of ϕ_1 and ϕ_2 in this scenario to that in the pair pro-

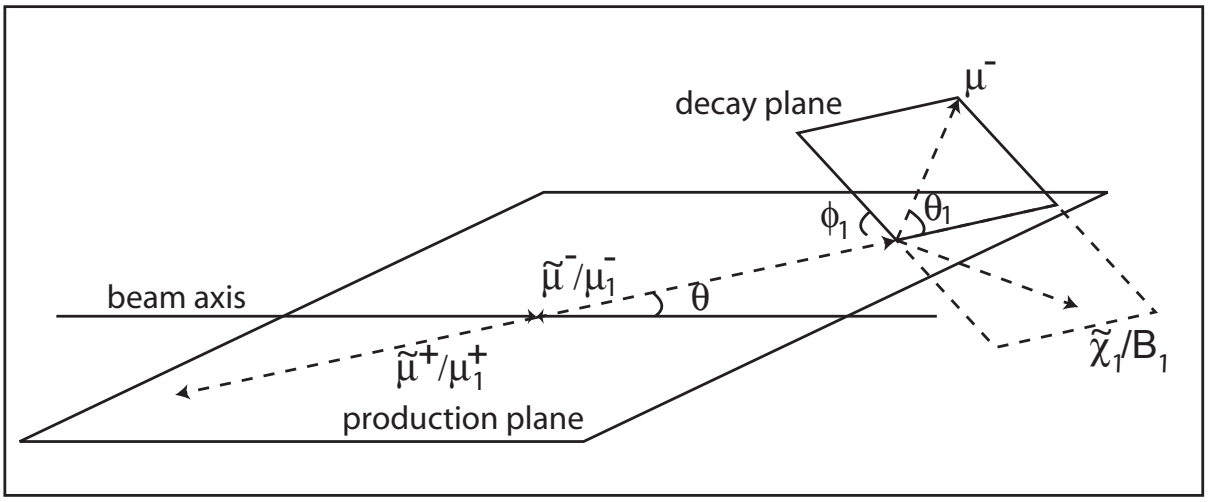

Figure 3.2: The pair-produced $\tilde{\mu}$ or μ_1 in the lab frame. The beam axis is defined as the z axis, with the production angle θ in the $x-z$ plane. The $\hat{z}$ axis is defined to point along the production axis. The decay angle ϕ_1 is invariant to boosts along $\hat{z}$, and so may be defined in either the lab frame or the frame of the decaying particle. The angle θ_1 is defined in the rest frame of $\tilde{\mu}^-/\mu_1^-$. Decay angles θ_2 and ϕ_2 (not shown) are defined equivalently for the $\tilde{\mu}^+/\mu_1^+$.

duction of μ_{1R}s decaying to muons and LKP B_1s in a UED model ($e^-e^+ \to \mu_{1R}^-\mu_{1R}^+ \to \mu^-\mu^+B_1B_1$). The Feynman diagrams for these processes are shown in Fig. 3.1. Analytic formulae for the production and decay cross sections for both models are presented in Appendix 3.6. We stress that SUSY and UED are chosen only as benchmark models with differing spins and similar final states; the method used to determine spin can in principle work equally well for any other scenario.

Representative spectra are required for both supersymmetry and universal extra dimensions. In addition, we wish to avoid any possible model-specific effects on the azimuthal distributions arising from different choices of spectra for supersymmetry and extra dimensions. Therefore, as the masses of the $\tilde{\mu}/\mu_1$ and $\tilde{\chi}_1^0/B_1$ are assumed to be known, we perform our analysis twice for each model. In the first case we assign the masses of the μ and B partners as per a SUSY spectrum, and then repeat the processes with the UED case.

As a representative supersymmetry point, we chose SPS 3 [44][45] in mSUGRA parameter space, which has $m_0 = 90$ GeV, $m_{1/2} = 400$ GeV, $A_0 = 0$, $\tan\beta = 10$, and a positive μ parameter. The universal extra dimensions model is represented by the minimal version (MUED) [46], which requires only four parameters: the number and radius R of the extra dimensions, the scale Λ to set flavor-universal boundary terms equal to zero, and the Higgs mass. We chose one extra dimension with $R^{-1} = 300$ GeV, $\Lambda = 20R^{-1}$ and a Higgs mass of 120 GeV. The resulting particle spectra at the TeV scale are shown in Table 3.1.

Backgrounds consist of the SM production of W^-W^+ pair production with leptonic decays to muons and neutrinos, ZZ production with decays to muons and neutrinos, and model-background of $\tilde{\chi}_1^+\tilde{\chi}_1^-/W_1^+W_1^-$ production decaying to muons and $\tilde{\nu}/\nu_1$. While kinematic cuts on the invariant mass of the muon pairs can greatly reduce the SM background, more efficient cuts can be obtained by requiring successful reconstruction of the $\tilde{\mu}_R/\mu_{1R}$ momentum as outlined in Appendix 3.5.

	SPS 3	MUED
$\tilde{\chi}_1^0/B_1$	161 GeV	302 GeV
$\tilde{\ell}_R/\ell_{1R}$	181 GeV	304 GeV
$\tilde{\ell}_L/\ell_{1L}$	289 GeV	309 GeV
$\tilde{\chi}_1^\pm/W_1^\pm$	306 GeV	327 GeV
$\tilde{\nu}_\ell/\nu_{1\ell}$	276 GeV	309 GeV

Table 3.1: Relevant particle spectra for the mSUGRA parameter point SPS 3 and the minimal universal extra dimension parameters $R^{-1} = 300$ GeV, $\Lambda = 20R^{-1}$, and $m_H = 120$ GeV. The MUED spectrum was derived using the MUED package [47] for CalcHEP [48]. Here, ℓ refers to the light charged leptons: electrons or muons.

The reconstruction algorithm assumes that the masses of the produced and escaping particles are known. By assuming that the signature of $\mu^-\mu^+\not{E}$ arises from pair production of $\tilde{\mu}_R$ (or μ_{1R}) decaying to LSP or LKP, all other events with the same signature but different particle masses develop inconsistencies in their reconstruction. That is, the visible momenta are not compatible with the pair production of particles with masses other than that for the $\tilde{\mu}_R/\mu_{1R}$ decaying into particles with masses other than that of the LSP/LKP. In practice, the parameter y defined in Eq. (3.17) becomes imaginary.

With perfect knowledge of masses and muon momentum, requiring reconstruction to succeed cuts nearly all of the background events. Once detector smearing and mass measurement errors are included, it is inevitable that some background will survive the reconstruction cut. Again, with the small errors in mass measurements available at the ILC, we do not expect large backgrounds to pollute the data set.

The total center-of-mass energy at the ILC is expected to reach up to 1 TeV, and an integrated luminosity of 500 fb^{-1} is not unrealistic. For the mass spectra chosen, the resulting cross sections times branching ratios are shown in Fig. 3.3 for $\sqrt{s}$ running from threshold up to 1 TeV. As a result, we expect several thousand to several hundreds of thousands of events available.

To simulate the effects of necessary cuts due to the geometry of the detector, we place cuts on the pseudo-rapidity η. We require η to be less than 2.5 for both visible muons, as otherwise the leptons would vanish unseen down the beam. Also, if the missing momentum also points down the beam pipe, we cannot be sure that the missing energy is truly in the form of WIMPs and not merely unobserved SM particles, so we cut on η for missing $\vec{p}_T$ as well.

Using HELAS [34] the production and decay matrix elements were calculated at tree level for each helicity state. Using the narrow-width approximation, the cross sections as a function of θ, ϕ_1, θ_1, ϕ_2, and θ_2 were obtained. BASES [35], an adaptive Monte Carlo program, was used to integrate over the other kinematic angles to determine the differential cross sections with respect to ϕ_1 and ϕ_2. As both decaying particles have the same spin statistics, the differential distributions are the same for both ϕ_1 and phi_2; hence, to increase statistics, the distributions for ϕ_1 and ϕ_2 were added.

Representative distributions for scalars and spinors (including rapidity cuts) are shown in Fig. 3.4. As can be clearly seen in Fig. 3.4a, both the true and false UED distributions have a clear $\cos\phi$ dependence, as expected from spinor decay (Eq. (3.5)). The true distributions for the scalar SUSY decay in Fig. 3.4b is flat, as expected from Eq. (3.4). It is therefore apparent even at this level of analysis that the ϕ dependence of the distribution contains the spin information necessary for our method.

Considering the combined true and false distribution in Fig. 3.4, a systematic issue for our

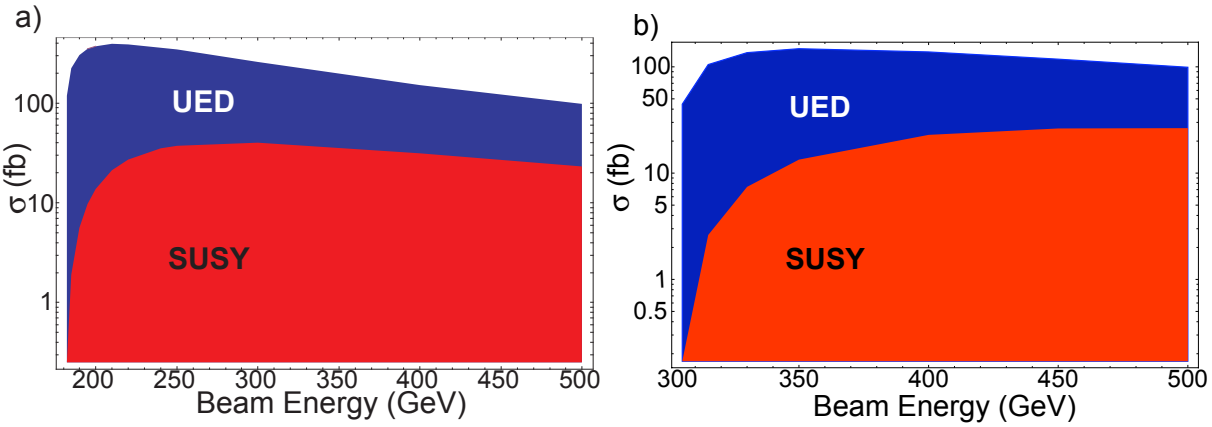

Figure 3.3: Cross sections times branching ratios as a function of the beam energy for the UED process $e^-e^+ \to \mu^-_{1R}\mu^+_{1R} \to \mu^-\mu^+ B_1 B_1$ and the SUSY process $e^-e^+ \to \tilde{\mu}^-_R\tilde{\mu}^+_R \to \mu^-\mu^+\tilde{\chi}^0_1\tilde{\chi}^0_1$. Figure a) uses the SPS 3 spectrum, while b) uses the MUED spectrum (see Table 3.1).

method becomes readily apparent. An unexpected $\cos 2\phi$ dependence develops due to the false distribution and rapidity cuts, a situation we regard as an indication of practical limitations to our method, not a fundamental flaw. Whereas the $\cos 2\phi$ dependence may be unimportant for the discrimination of scalar versus higher spin states, it will become important in distinguishing spinor from vectors (section 3.3). Though harder to see by eye, the UED distribution also develops a $\cos 2\phi$ dependence in the false solution. As such, we fit not to $A_0 + A_1 \cos\phi$ but rather to $A_0 + A_1 \cos\phi + A_2 \cos 2\phi$.

The overall scaling of the A_i parameters in Eqs. (3.4), (3.5), and (3.6) depends on the total number of events, which is a function of the total cross section. To remove this model-dependent effect, the parameter of interest in spin determination is not A_1, but A_1/A_0, which is independent of the scaling due to total cross section.

Using the least-squares method the generated distributions were fit to $A_0 + A_1 \cos\phi + A_2 \cos 2\phi$. The errors for each parameter A_i were obtained after marginalizing over the other two parameters. The ratio A_1/A_0 for the scalar $\tilde{\mu}_R$ and spinor μ_{1R} are shown in Fig. 3.5. As can be seen, for both the SPS3 and MUED spectra the values of A_1/A_0 for $\tilde{\mu}_R$ are consistent with zero for all energies and for both the true and false distributions. For the spinor μ_{1R}, the ratio is manifestly nonzero, allowing us to distinguish scalars from higher spin states.

Several aspects of Fig. 3.5 require closer examination. The large error bars for the supersymmetric particles in both spectra are due to the relatively poor statistics compared to the pair production of the spinor KK modes in universal extra dimensions. This is especially apparent near threshold. For the spinor particles we also note that, near threshold, the signal is on the order of 10%, and decreases toward zero at progressively higher energies. This decrease can be readily explained as follows: far from threshold, the mass of the pair-produced particles becomes less relevant, and so their spins become more correlated due to chirality conservation. To determine the distribution of ϕ_1 (ϕ_2), we integrate over all other angles in the problem, including ϕ_2 (ϕ_1). Due to the correlation of spins in this energy regime, this integration results in decoherence of the sum of matrix elements. That is, rather than considering $|\sum_h \mathcal{M}(h)|^2$, at high energies the cross section becomes proportional to $\sum_h |\mathcal{M}(h)|^2$, which has no azimuthal angle dependence due to the lack of interference between terms.

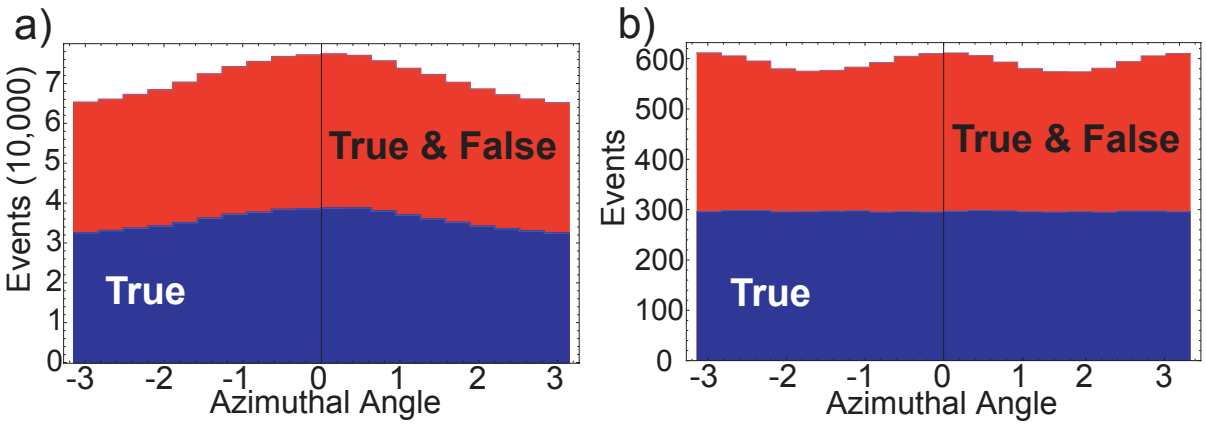

Figure 3.4: Histograms of number of events per azimuthal angle ϕ for both the true solution to the reconstruction algorithm and the combined true and false distribution. The center-of-mass energy is $\sqrt{s} = 370$ GeV and the luminosity if 500 fb^{-1}. Figure a) shows the UED distribution for $e^-e^+ \to \mu^-_{1R}\mu^+_{1R} \to \mu^-\mu^+ B_1 B_1$ while b) is the SUSY distribution for $e^-e^+ \to \tilde{\mu}^-_R\tilde{\mu}^+_R \to \mu^-\mu^+\tilde{\chi}^0_1\tilde{\chi}^0_1$.

Finally, in considering the distribution of true solutions versus that of the combined solutions, we note that for the spinor case the signal is lower once the false solutions are added in. At low energies the difference between the two is comparatively small, but grows as we move away from threshold. This agrees well with the naive intuition that the false distribution should be flat in ϕ_1 and ϕ_2; however, we stress that at higher frequencies such intuition fails us, and the flat distribution may develop nontrivial $\cos 2\phi$ dependences.

To demonstrate this effect, we plot in Fig. 3.6 the ratio A_2/A_0 for the decay of spinor μ_{1R} (using SPS3 parameters). As can be seen in the top plot, the true solution without cuts has a coefficient of zero for the $\cos 2\phi$ term, as predicted by Eq. (3.5) for spinor decay. However, once cuts and the false solutions are added, a nonzero value is generated. Clearly, this can cause confusion between a spin-1/2 particle and a vector or higher spin state.

To attempt to correct for this effect, we generate events in which the particles decay according to phase space. This flat distribution is reconstructed using the method outlined in Appendix 3.5 and rapidity cuts are applied just as in the SUSY and UED cases. As a result, the flat distributions also develop a $\cos 2\phi$ dependence. The resulting values for A_2/A_0 using only true solutions (with and without cuts) and then both solutions (with and without cuts) are subtracted from the appropriate spinor ratios to isolate the spin-dependent effect. The resulting corrected A_2/A_0 values are displayed in the lower plot in Fig. 3.6. As can be seen, the flat distribution corrects the $\cos 2\phi$ contribution due to cuts but does not remove the false distribution's effect, leaving a $\sim 0.5\%$ spurious signal at high energies. For reasons we do not yet fully appreciate, at low energies the false distribution's effects are minimal, allowing for the possibility of accurate spin measurements. However, it is exactly in this regime that statistics are poor due to the proximity of the threshold.

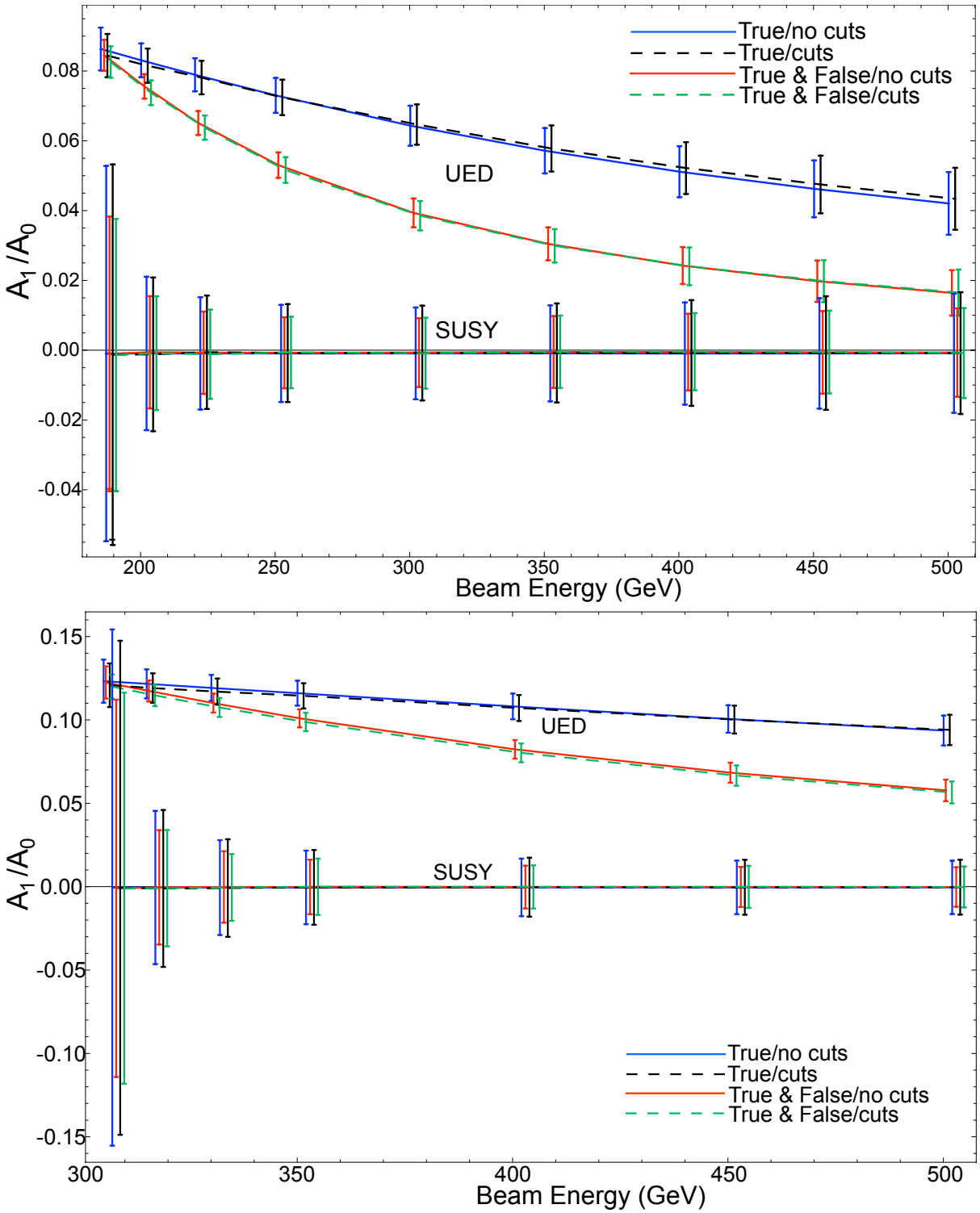

Figure 3.5: Top: Ratio A_1/A_0 for mSUGRA parameter point SPS3 as a function of energy for both scalar (SUSY) and spinor (UED) pair production with 500 fb^{-1} luminosity.. Error bars correspond to 95% exclusion region. Blue lines correspond to true solution only with no rapidity cuts, black dashed lines are true solutions with rapidity cuts, red lines are true and false solutions without cuts, and green are true and false solutions with cuts. Bottom: Ratio A_1/A_0 for MUED parameters as in Table 3.1 for both scalar (SUSY) and spinor (UED) production. Color labeling identical to the above.

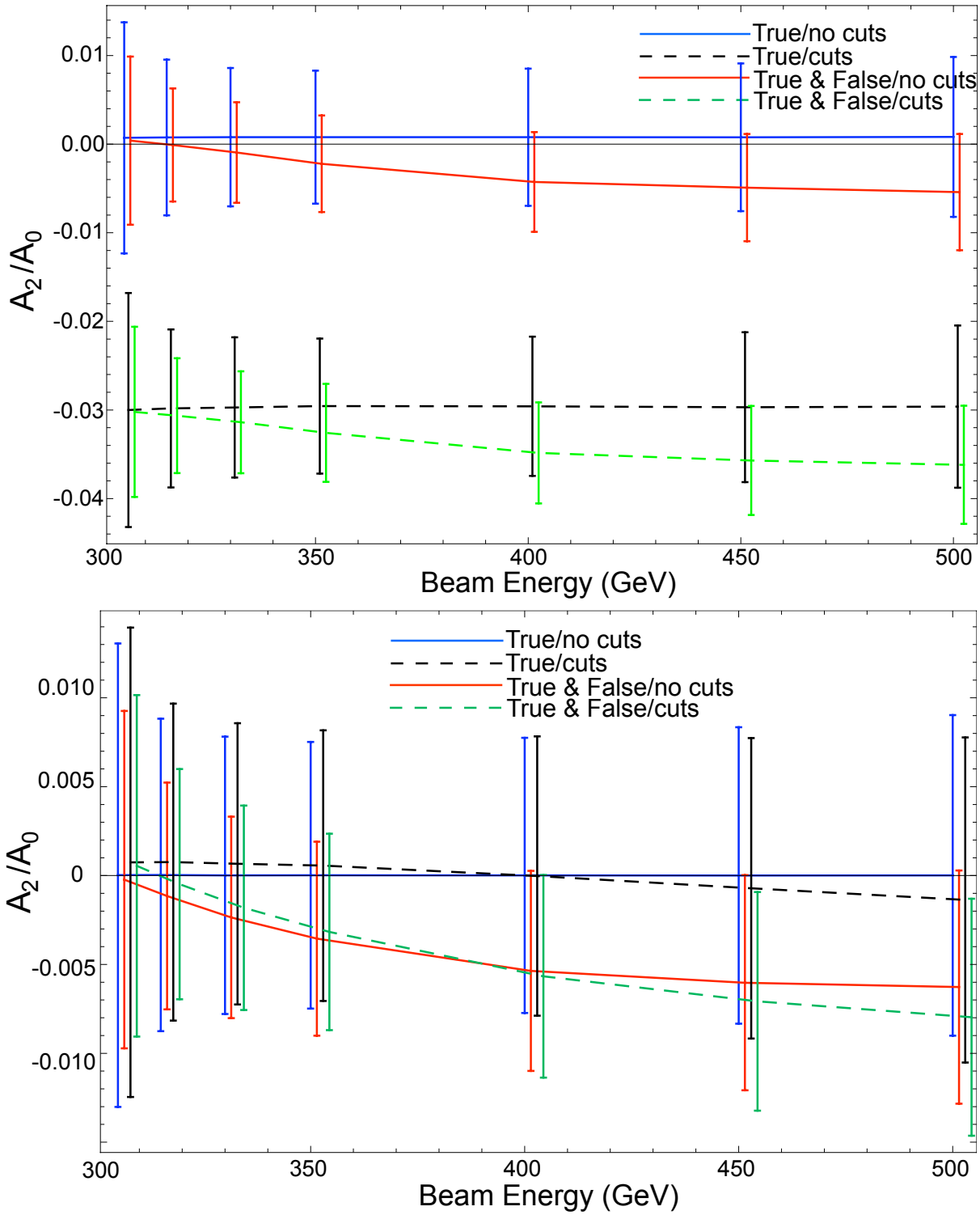

Figure 3.6: Top: Ratio A_2/A_0 for mSUGRA parameter point SPS3 as a function of energy for spinor (UED) pair production with 500 fb^{-1} luminosity. Error bars correspond to 95% exclusion region. Blue lines correspond to true solution only with no rapidity cuts, black dashed lines are true solutions with rapidity cuts, red lines are true and false solutions without cuts, and green are true and false solutions with cuts. Bottom: Ratio A_2/A_0 for SPS3 parameters for spinor (UED) production after correcting for effects of false distribution and cuts on a flat distribution. Color labeling identical to the above.

3.3 Spinor vs. Vector

Due to the large A_1/A_0 signal for non-scalars (on the order of 10%) and the minimal effect of rapidity cuts and false distributions on this ratio, the ILC should have little difficulty discerning that a particle is spin-0. However for higher spins the cuts and false solutions introduce potentially dangerous higher frequency contributions, as has been demonstrated.

Consequently, the question still remains whether this method may be practically applied to discriminate spinors from vectors in general cases. We therefore consider a case of pair production of massive vector bosons in UED contrasted with spinor production in SUSY. In particular, we consider $e_L^- e_L^+ \to W_1^- W_1^+ \to \ell^- \ell'^+ \bar{\nu}_{1\ell} \nu_{1\ell'}$ in universal extra dimensions and $e_L^- e_L^+ \to \tilde{\chi}_1^- \tilde{\chi}_1^+ \to \ell^- \ell'^+ \tilde{\nu}_{\ell'}^* \tilde{\nu}_{\ell'}$ in supersymmetry where the leptons ℓ and ℓ' can be either muon or electron type (see Fig. 3.7). Even though the $\nu_1/\tilde{\nu}$ are not the LSP/LKP, they decay to neutrinos and the LSP, neither of which is visible in the detector.

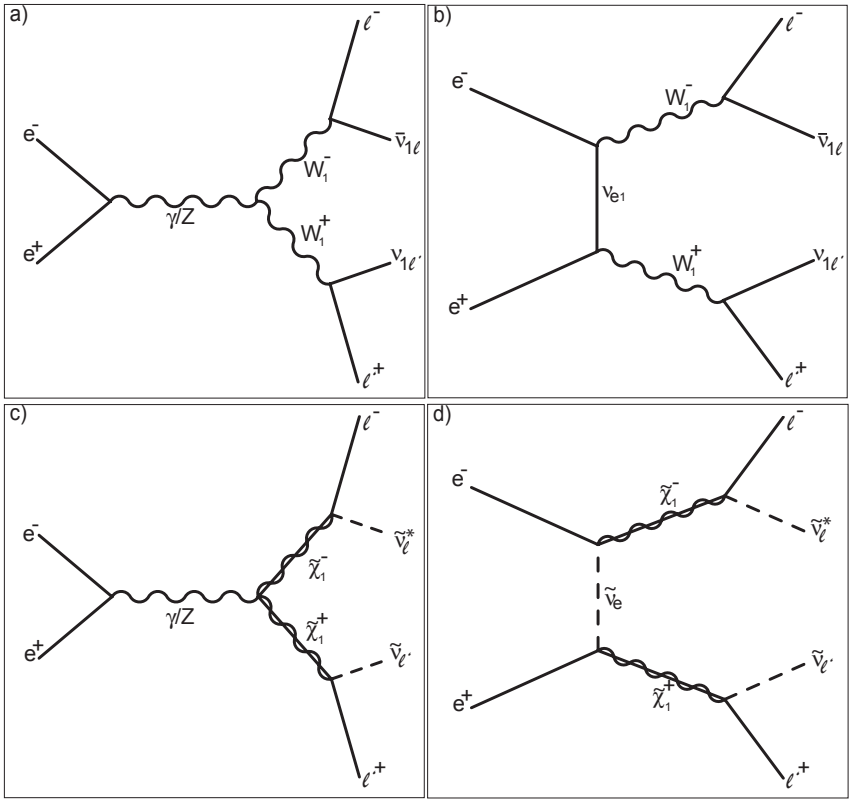

Figure 3.7: a) s-channel and b) t-channel pair production of KK$=1$ W bosons in universal extra dimensions decaying to opposite-sign leptons and missing energy in the form of two ν_1s. c) s-channel and d) t-channel pair production of charginos $\tilde{\chi}_1^\pm$ in supersymmetry decaying to opposite-sign leptons and sneutrino missing energy

For these final states, the total cross sections times branching ratios as a function of energy are shown in Fig. 3.8. Once again, the supersymmetric cross section is considerably less than that in extra dimensions. Furthermore, the small mass splittings in the MUED spectrum lead to small cross sections

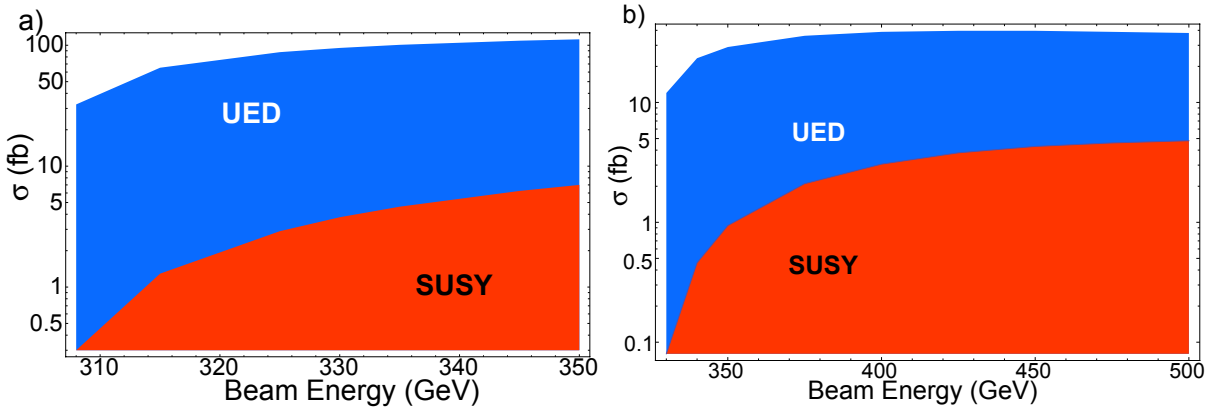

Figure 3.8: Cross sections times branching ratios as a function of beam energy for the UED process $e_L^- e_L^+ \to W_1^- W_1^+ \to \ell^- \ell'^+ \bar{\nu}_{1\ell} \nu_{1\ell'}$ and the SUSY process $e_L^- e_L^+ \to \tilde{\chi}_1^- \tilde{\chi}_1^+ \to \ell^- \ell'^+ \tilde{\nu}_{\ell'}^* \tilde{\nu}_{\ell'}$. Figure a) uses the SPS 3 spectrum, while b) uses the MUED spectrum (see Table 3.1).

compared to the SPS 3 case. Backgrounds include SM $W^\pm$ and ZZ production, and model backgrounds from $\tilde{\chi}_2^0 \tilde{\chi}_2^0 / W_1^3 W_1^3$, and $\tilde{\ell}^- \tilde{\ell}^+ / \ell_1^- \ell_1^+$ pair production decaying to charged leptons and missing energy. However, we once again find that demanding successful reconstruction effectively cuts the background to negligible levels. In addition, we apply the $\eta \leq 2.5$ cuts on the charged leptons and missing momentum.

We perform fits to $A_0 + A_1 \cos\phi + A_2 \cos 2\phi$ as in section 3.2 and consider the ratio A_2/A_0, using 1 ab^{-1} of integrated luminosity (due to the smaller cross sections). The results for the SPS3 spectrum are displayed in Fig. 3.9, and those of the MUED spectrum are shown in Fig. 3.10. Note that the true solutions for the vector bosons consist of an approximately 1% signal in the SPS3 spectrum and $\sim 0.5\%$ in MUED. In both spectra the true solution for spinors is consistent with zero. As with the production of μ_{1R}, however, the presence of the false distribution introduces significant spurious values of A_2/A_0, dwarfing the true signal by a factor of ~ 5.

In the SPS3 spectrum, even with 1 ab^{-1} the error bars on the true solution for the vector bosons barely exclude zero at 95% confidence. For the MUED case, the situation is much worse, as a smaller signal is combined with cross sections suppressed by nearly an order of magnitude compared to those in the SPS3 case. Thus, statistics may be a limiting factor in measuring nonzero spins.

We attempt to correct for the effects of cuts and false solutions by generating events which decay according to phase space. As the production angle may be measured up to the two-fold reconstruction ambiguity, we generate the particles with the correct θ distributions and flat θ_i, ϕ_i distributions and run the resulting events through the reconstruction and detector simulator. The resulting values for A_2/A_0 are subtracted from those in Figs. 3.9 and 3.10 in an attempt to isolate the spin effects arising from quantum interference from the nonzero A_2/A_0 coming from cuts and the false solutions. The adjusted results are shown in Fig. 3.11 for the SPS3 spectrum. Due to the small signal and poor statistics in the MUED spectrum, even the uncorrected signal in the true solution cannot be distinguished from zero, so we do not adjust for cuts or the false solutions.

Examining Fig. 3.11, we find that the flat distribution captures the effects of cuts on the ratio A_2/A_0 but does not correctly account for the false distributions. We do find that the false distributions do not contribute significantly to the ratio near threshold, as in the measurements of A_1/A_0. Once again, this behavior is not well understood and statistics in this regime are limited. It is conceivable that better

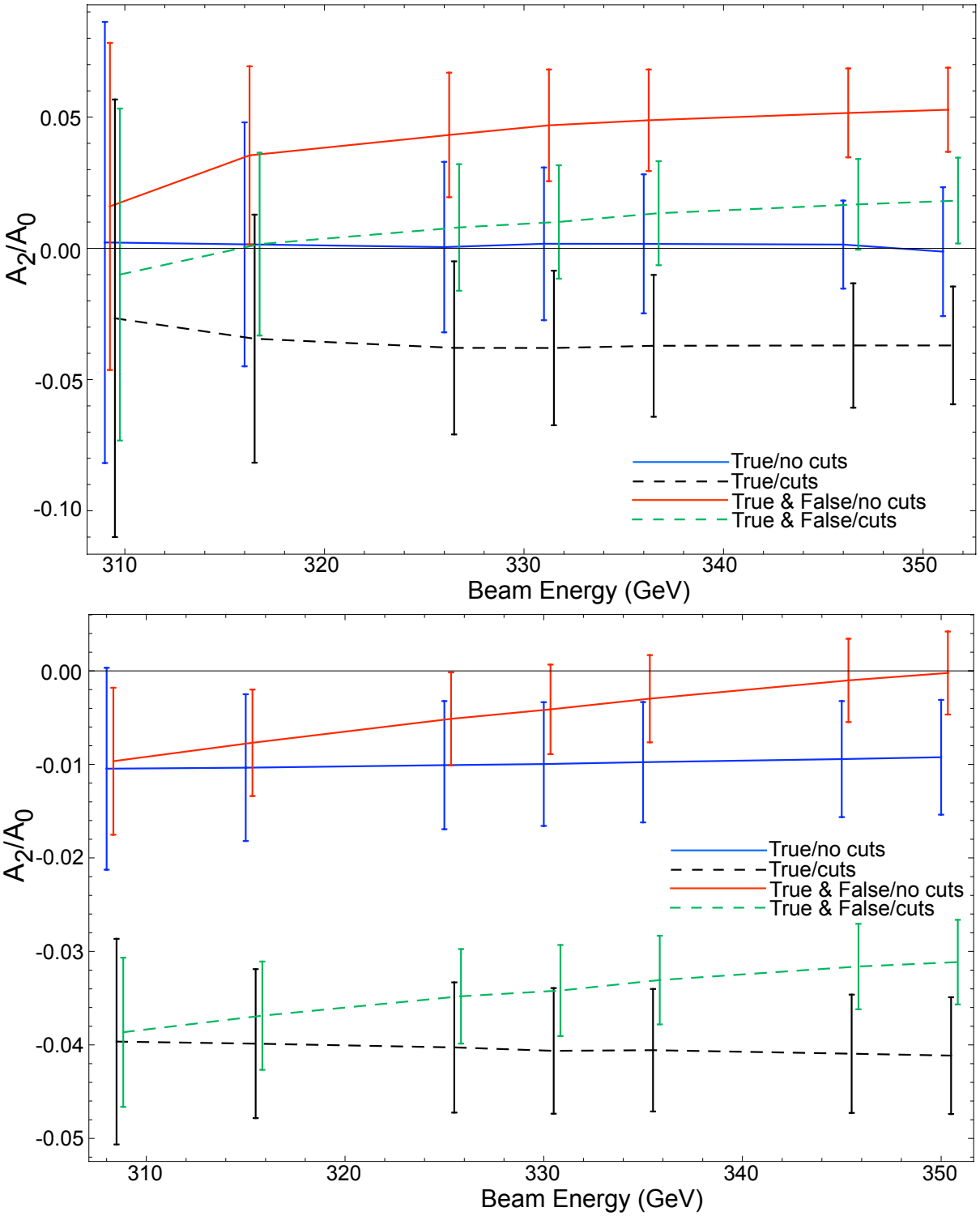

Figure 3.9: Top: Ratio A_2/A_0 versus beam energy for the supersymmetric spinor production $e_L^- e_L^+ \to \tilde{\chi}_1^- \tilde{\chi}_1^+ \to \ell^- \ell'^+ \tilde{\nu}_\ell^* \tilde{\nu}_{\ell'}$ for the SPS3 spectrum. Bottom: Ratio A_2/A_0 for the UED vector boson production $e_L^- e_L^+ \to W_1^- W_1^+ \to \ell^- \ell'^+ \bar{\nu}_{1\ell} \nu_{1\ell'}$ for the same spectrum. Color coding as in Fig. 3.5. Error bars correspond to 95% exclusion region assuming 1 ab^{-1} luminosity.

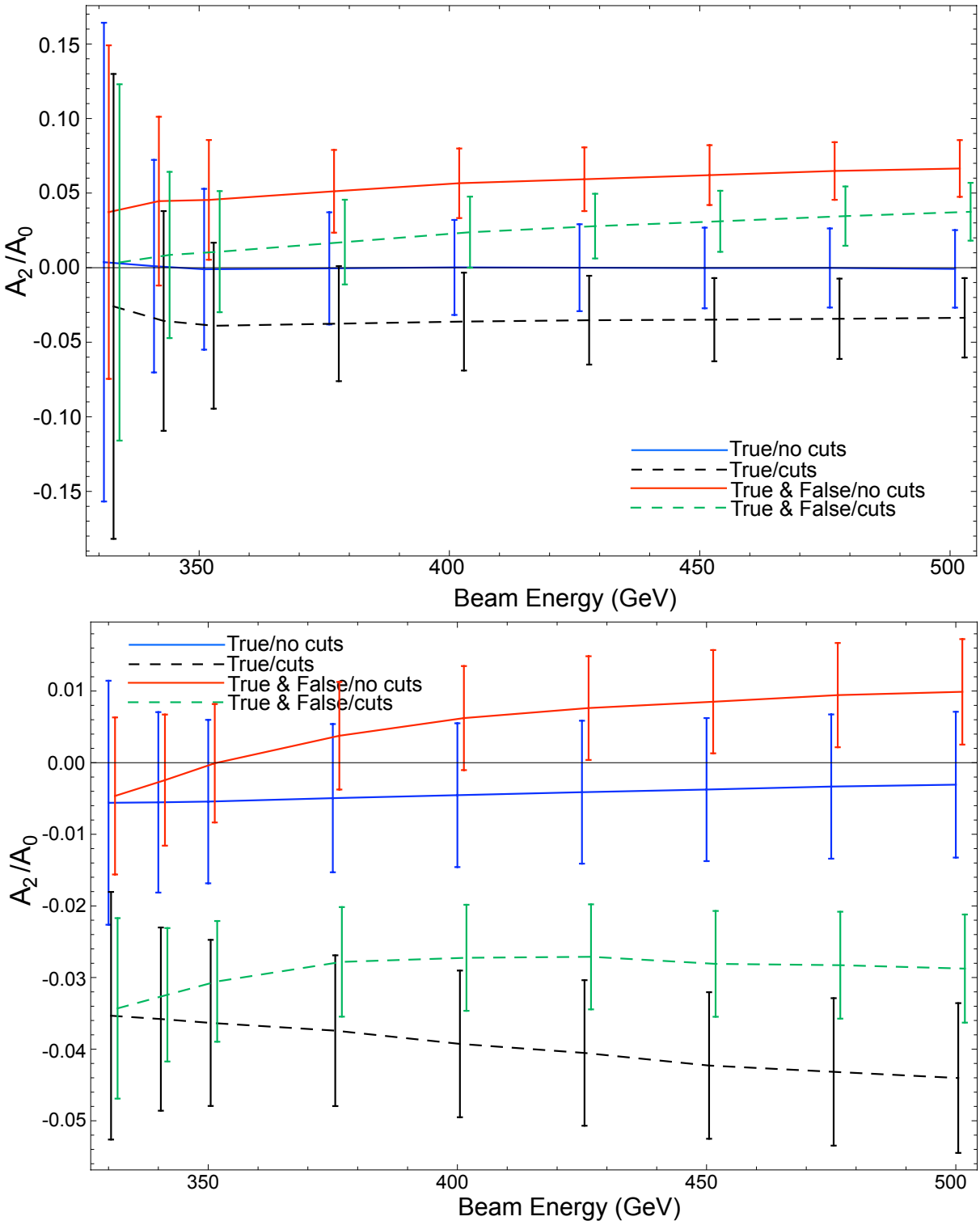

Figure 3.10: Top: Ratio A_2/A_0 versus beam energy for the supersymmetric spinor production $e_L^- e_L^+ \to \tilde{\chi}_1^- \tilde{\chi}_1^+ \to \ell^- \ell'^+ \tilde{\nu}_{\ell'}^* \tilde{\nu}_{\ell'}$ for the MUED spectrum (see Table 3.1). Bottom: Ratio A_2/A_0 for the UED vector boson production $e_L^- e_L^+ \to W_1^- W_1^+ \to \ell^- \ell'^+ \bar{\nu}_{1\ell} \nu_{1\ell'}$ for the same spectrum. Color coding as in Fig. 3.5. Error bars correspond to 95% exclusion region assuming 1 ab^{-1} luminosity.

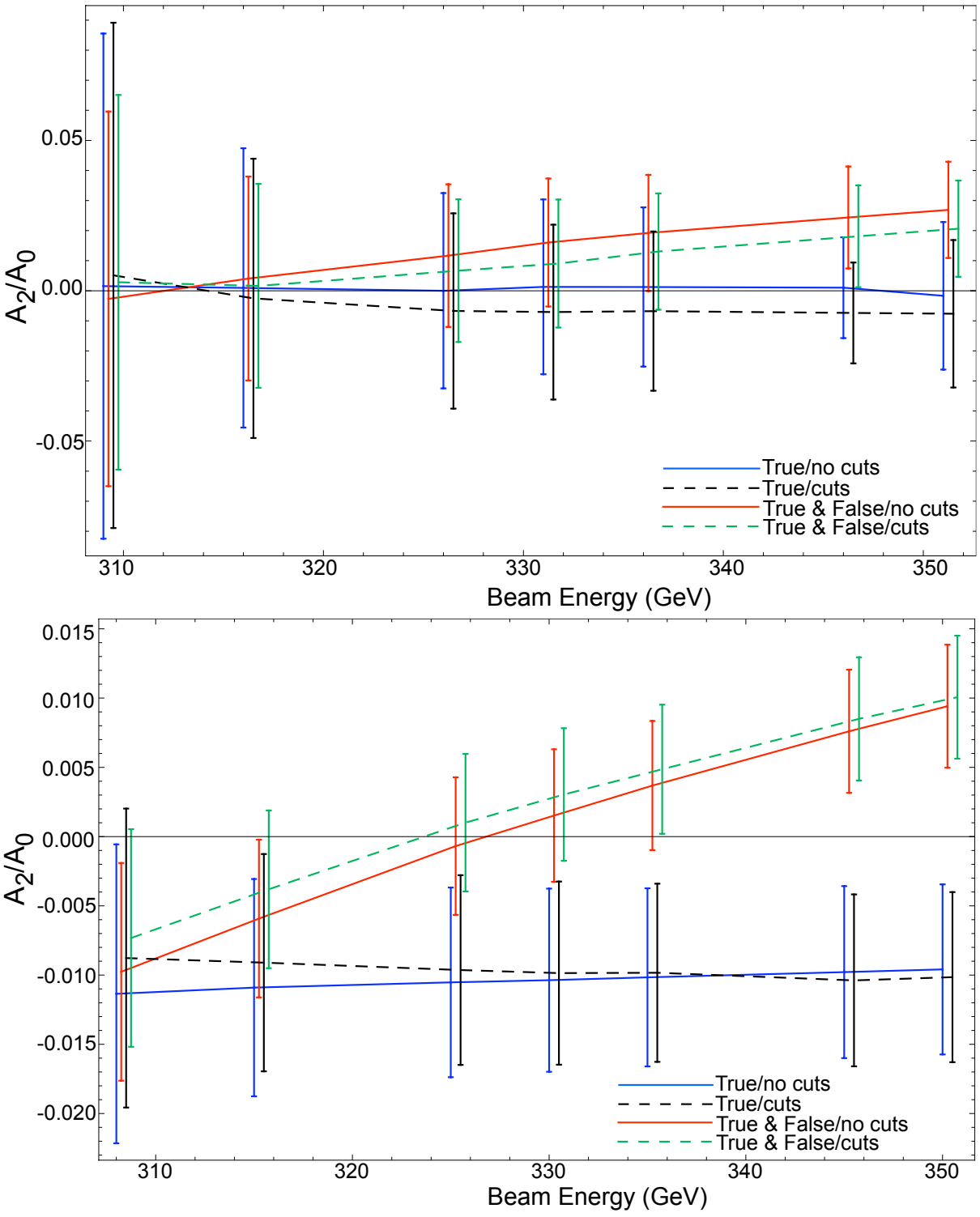

Figure 3.11: Top: Ratio A_2/A_0 versus beam energy for the supersymmetric spinor production $e_L^- e_L^+ \to \tilde{\chi}_1^- \tilde{\chi}_1^+ \to \ell^- \ell'^+ \tilde{\bar{\nu}}_{\ell'} \tilde{\nu}_{\ell'}$ for the SPS3 spectrum adjusted to account to detector and cut effects. Bottom: Ratio Adjusted values of A_2/A_0 for the UED vector boson production $e_L^- e_L^+ \to W_1^- W_1^+ \to \ell^- \ell'^+ \bar{\nu}_{1\ell} \nu_{1\ell'}$ for the same spectrum. Color coding as in Fig. 3.5. Error bars correspond to 95% exclusion region assuming 1 ab^{-1} luminosity.

results would be obtained by coupling a flat decay in ϕ_i with the *measured* distribution of θ_i to attempt to account for the false distribution. This matching has not been performed as yet.

Thus, while the quantum interference measurement for spin-0 stands on solid ground, the situation for higher spins is less certain. Even neglecting the issue of false solutions, the vector boson ratio A_2/A_0 is on the order of 1%, and so requires significant statistics in order to distinguish from spinor decays. Furthermore, the false distribution introduces a spurious A_2/A_0 value which has not been fully understood by the authors and can dwarf the signal. Finally, the case of the MUED spectrum demonstrates that, while the method of spin measurement is model independent, it is vulnerable to model-dependent effects such as total cross section, which control the statistical error of the fit. However, note that we could do much better statistically by adding hadronic final states for one of the $\tilde{\chi}_1^{\pm}/W_1$ while requiring leptonic final states for the other. We again would have two-fold ambiguity, but the rest of the measurement remains the same as long as we can measure the hadronic energies well enough. This may be possible by using the energy flow method that matches tracking and calorimeter information.

3.4 Conclusions

We have demonstrated that the quantum interference of multiple helicity states can provide a model independent method of spin measurements at the ILC. Specifically, with reasonable luminosities, scalar particles can be easily distinguished from spin-1/2 or higher possibilities in pair production followed by decays to visible leptons and missing energy.

Determining whether a particle is spin-1/2 or spin-1 suffers from two major problems. The first is simply statistics: as the signal is on the order of 1%, the requisite luminosity will be a stretch for the ILC, at least in the SUSY and UED models considered. The second issue concerns the false solution to the reconstruction of the pair-produced particles' 4-momentum, and hence the derived values of the azimuthal angles ϕ_1 and ϕ_2. With 8 missing momentum components from the two weakly interacting particles escaping the detector, 4 measured total missing momenta, and 4 mass constraints, the system can be solved only up to a two-fold ambiguity. While the $\cos\phi$ distribution is flat in the false solution, non-trivial dependences on $\cos 2\phi$ develop. From explicit calculations, these dependences appear to be different for flat, spinor, and vector boson distributions, and so cannot be subtracted from the combined solutions without losing the desired model-independence.

It therefore behooves us to consider methods for full reconstruction of the event. If the decay proceeds by emitting several visible particles in a cascade of particles with known mass down to the LSP/LKP, then we may overconstrain the decay, allowing for full reconstruction. In particular, if the pair-produced particles decay to the LSP through an intermediate state, then there would be 6 mass constraints on the system. With only 8 unknown quantities and 4 measured values, the false solution is no longer present. Unfortunately, all such decays considered by the authors so far have too low a cross section to provide useful spin measurements.

However, such lengthy decay chains raises the possibility of applying this method to the LHC. At a hadron collider the center-of-mass energy and frame of reference are unknown for a particular parton-parton level event. Thus, only 2 measured quantities may be obtained in the event: the components of missing transverse momentum $\not{p}_T$. With a multi-step decay we obtain 6 mass constraints and, combining these with the measured $\not{p}_T$ we can solve the system of 8 missing momentum components up to the two-fold ambiguity. Additionally, the reconstruction algorithm can be used in a modified form [38] to measure the masses in the decay chain as a necessary preliminary step to determining the azimuthal

angles. As the cross section for producing TeV-scale particles with color charge at the LHC is very large (e.g., ~ 1 pb for $\tilde{g}$ or $\tilde{q}$ pair production [49]), it seems likely that we may obtain enough statistics in such a case to at least measure the spin of scalar particles, if not those of spin 1 or 1/2. This may possibly allow discrimination between the gluino and the KK gluon.

Note that the method we proposed can be used and tested already in the Tevatron top-quark sample. The interference between the two helicity states of the top quark should give rise to $\cos\phi$ dependence. For the lepton+jet mode, one can fully reconstruct the event without a two-fold ambiguity, but this suffers from W+multi-jet background and the less than stellar jet energy resolution. The purely leptonic mode has two-fold ambiguity but less background and better momentum resolution. Run-II should already have enough statistics to attempt the study of azimuthal distributions, giving the first direct experimental hint on the spin-$1/2$ nature of the top quark.

3.5 Reconstruction

The two charged leptons in the events shown in Fig. 3.1 have momenta p_1 and p_2, respectively. We define the perpendicular momentum in the event $\vec{p}_\perp = \vec{p}_1 \times \vec{p}_2$. We refer to the pair-produced unstable particles as A (for μ^-_{1R} or $\tilde{\mu}^-_R$) and B (μ^+_{1R} or $\tilde{\mu}^+_R$). The missing 4-momentum from the decay of A is $\not{p}_1$, while $\not{p}_2$ is the missing momentum from the decay of B. Both the particles escaping the detector have mass m, which is assumed to be known.

Since the pair-produced particles A and B (with mass M) are back to back, it suffices to solve for p_A, as $\vec{p}_A = -\vec{p}_B$. The final-state leptons are effectively massless, so $p_1^2 = p_2^2 = 0$. For the massive particles, we have

$$\begin{aligned} p_A^2 &= p_B^2 = M^2 && (3.7)\\ \not{p}_1^2 &= \not{p}_2^2 = m^2. && (3.8) \end{aligned}$$

Finally, since p_A (p_B) decays into $\not{p}_1$ ($\not{p}_2$) and p_1 (p_2),

$$\begin{aligned} \not{p}_1 &= p_A - p_1 \\ \not{p}_2 &= p_B - p_2. && (3.9) \end{aligned}$$

At the ILC, the energy of the beams E is known, and for pair production the total energy in the event must be split equally, so $p_A^0 = p_B^0 = E$. Therefore, using Eqs. (3.7), (3.8), and (3.9) we may define the following variables:

$$\begin{aligned} c_1 &\equiv \vec{p}_A \cdot \vec{p}_1 = \frac{1}{2}(m^2 - M^2 + 2Ep_1^0) && (3.10)\\ c_2 &\equiv \vec{p}_A \cdot \vec{p}_2 = -\frac{1}{2}(m^2 - M^2 + 2Ep_2^0) && (3.11)\\ b_2 &\equiv \vec{p}_A \cdot \vec{p}_A = E^2 - M^2 && (3.12)\\ a_{ij} &\equiv \vec{p}_i \cdot \vec{p}_j \ (i,j = 1,2). && (3.13) \end{aligned}$$

We can write the momentum $\vec{p}_A$ as

$$\vec{p}_A = t_1\vec{p}_1 + t_2\vec{p}_2 + y\vec{p}_\perp. \qquad (3.14)$$

Using this definition in Eq. (3.10) and (3.11), we find

$$\begin{aligned} c_1 &= t_1 a_{11} + t_2 a_{12} \\ c_2 &= t_1 a_{12} + t_2 a_{22} \\ t_1 &= \frac{a_{22} c_1 - a_{12} c_2}{a_{11} a_{22} - a_{12}^2} \qquad (3.15) \\ t_2 &= \frac{a_{11} c_2 - a_{12} c_1}{a_{11} a_{22} - a_{12}^2}. \qquad (3.16) \end{aligned}$$

Finally, using Eqs. (3.12), (3.15), and (3.16), we have

$$\begin{aligned} b_2 &= (t_1^2 a_{11} + 2 t_1 t_2 a_{12} + t_2^2 a_{22}) + y |\vec{p}_\perp|^2 \\ y &= \pm \sqrt{\frac{b_2 - (t_1^2 a_{11} + 2 t_1 t_2 a_{12} + t_2^2 a_{22})}{|\vec{p}_\perp|^2}}. \qquad (3.17) \end{aligned}$$

The $\pm$ sign in this last equation is the two-fold ambiguity in the reconstruction.

3.6 Amplitudes

The matrix elements for right-handed smuon pair production from polarized $e^- e^+$ beams are

$$\begin{aligned} \mathcal{M}(e_L^- e_R^+ \to \tilde{\mu}_R^- \tilde{\mu}_R^+) &= (-ie^2) \sqrt{1 - \frac{4m_{\tilde{\mu}}^2}{s^2}} \sin\theta \times \\ &\left(1 + \frac{s(-1/2 + s_W^2)}{c_W^2 (s - 4m_Z^2)}\right) \qquad (3.18) \\ \mathcal{M}(e_R^- e_L^+ \to \tilde{\mu}_R^- \tilde{\mu}_R^+) &= (-ie^2) \sqrt{1 - \frac{4m_{\tilde{\mu}}^2}{s^2}} \sin\theta \times \\ &\left(1 + \frac{s_W^2 s}{c_W^2 (s - 4m_Z^2)}\right). \end{aligned}$$

Here, $\sqrt{s}$ is the center-of-mass energy and $m_{\tilde{\mu}}$ is the mass of the right-handed smuon. The angle θ is defined as in Fig. 3.2.

The decaying $\tilde{\mu}^\pm$ goes to $\mu_R^\pm$ and a right-handed $\tilde{\chi}_1^0$. We make the approximation that the neutralino is primarily bino, and so the decay matrix element is

$$\mathcal{M}(\tilde{\mu}^\pm \to \mu^\pm \tilde{\chi}_1^0) = -\sqrt{2} g' \sqrt{m_{\tilde{\mu}}^2 - m_{\tilde{\chi}}^2}, \qquad (3.19)$$

where g' is the hypercharge gauge coupling $g' = \frac{e}{\cos\theta_w}$. Making the narrow-width approximation, the cross section for the four-body final state is simply the incoherent sum over initial helicities,

$$\begin{aligned} d\sigma &= \frac{d\Phi_4}{4} \sum_{L,R} \Big| \mathcal{M}(e_{L/R}^- e_{R/L}^+ \to \tilde{\mu}^- \tilde{\mu}^+) \mathcal{M}(\tilde{\mu}_R^- \to \mu_R^- \tilde{\chi}_1^0) \times \\ &\quad \mathcal{M}(\tilde{\mu}_R^+ \to \mu_R^+ \tilde{\chi}_1^0) \Big|^2 2\pi\delta(s_{\mu^+ \tilde{\chi}_1^0} - m_{\tilde{\mu}}^2) \times \\ &\quad 2\pi\delta(s_{\mu^- \tilde{\chi}_1^0} - m_{\tilde{\mu}}^2) \frac{1}{(2 m_{\tilde{\mu}} \Gamma)^2}, \qquad (3.20) \end{aligned}$$

where Γ is the total width of the $\tilde{\mu}_{1R}$. Note the lack of dependence on ϕ_1 and ϕ_2, in accordance with Eq. (3.4).

Pair production for right-handed μ_1 requires four helicity combinations for the μ_{1R}s. Recall that KK states of the chiral muons are massive particles, and as such they can have either helicity. Thus, the production matrix elements are

$$\begin{aligned}
\mathcal{M}(e_L^- e_R^+ \to \mu_{1R}^-(\downarrow)\mu_{1R}^+(\uparrow)) &= (ie^2)(1-\cos\theta)\times \\
&\quad \left(1+\frac{s(-1/2+s_W^2)}{c_W^2(s-m_Z^2)}\right) \\
\mathcal{M}(e_R^- e_L^+ \to \mu_{1R}^-(\downarrow)\mu_{1R}^+(\uparrow)) &= (-ie^2)(1+\cos\theta)\times \\
&\quad \left(1+\frac{s_W^2 s}{c_W^2(s-m_Z^2)}\right) \\
\mathcal{M}(e_L^- e_R^+ \to \mu_{1R}^-(\downarrow)\mu_{1R}^+(\downarrow)) &= (-ie^2)\frac{2m_{\mu_1}}{\sqrt{s}}\sin\theta \\
&\quad \left(1+\frac{s(-1/2+s_W^2)}{c_W^2(s-m_Z^2)}\right) \\
\mathcal{M}(e_R^- e_L^+ \to \mu_{1R}^-(\downarrow)\mu_{1R}^+(\downarrow)) &= (-ie^2)\frac{2m_{\mu_1}}{\sqrt{s}}\sin\theta \\
&\quad \left(1+\frac{s_W^2 s}{c_W^2(s-m_Z^2)}\right) \\
\mathcal{M}(e_L^- e_R^+ \to \mu_{1R}^-(\uparrow)\mu_{1R}^+(\downarrow)) &= (-ie^2)(1+\cos\theta)\times \\
&\quad \left(1+\frac{s(-1/2+s_W^2)}{c_W^2(s-m_Z^2)}\right) \\
\mathcal{M}(e_R^- e_L^+ \to \mu_{1R}^-(\uparrow)\mu_{1R}^+(\downarrow)) &= (ie^2)(1-\cos\theta)\times \\
&\quad \left(1+\frac{s_W^2 s}{c_W^2(s-m_Z^2)}\right) \\
\mathcal{M}(e_L^- e_R^+ \to \mu_{1R}^-(\uparrow)\mu_{1R}^+(\uparrow)) &= (ie^2)\frac{2m_{\mu_1}}{\sqrt{s}}\sin\theta \\
&\quad \left(1+\frac{s(-1/2+s_W^2)}{c_W^2(s-m_Z^2)}\right) \\
\mathcal{M}(e_R^- e_L^+ \to \mu_{1R}^-(\uparrow)\mu_{1R}^+(\uparrow)) &= (ie^2)\frac{2m_{\mu_1}}{\sqrt{s}}\sin\theta \\
&\quad \left(1+\frac{s_W^2 s}{c_W^2(s-m_Z^2)}\right).
\end{aligned} \tag{3.21}$$

Here, $\uparrow$ corresponds to right-handed helicity, while $\downarrow$ is left-handed.

In the rest frame of the decaying μ_{1R}, there are two possible helicities ($\uparrow$ and $\downarrow$) decaying to right-handed muons and three possible polarization vectors for the B_1 (ϵ_λ, $\lambda = \pm 1, 0$). For the decay of

the μ_{1R}^-, the matrix elements are

$$\begin{aligned}
\mathcal{M}(\mu_{1R}^-(\uparrow) \to \mu_R^- B_1(-1)) &= 0 \\
\mathcal{M}(\mu_{1R}^-(\uparrow) \to \mu_R^- B_1(0)) &= g' \frac{m_{\mu_1}}{m_{B_1}} \sqrt{m_{\mu_1}^2 - m_{B_1}^2} \times \\
&\quad e^{+i\phi_1/2} \cos\frac{\theta_1}{2} \\
\mathcal{M}(\mu_{1R}^-(\uparrow) \to \mu_R^- B_1(+1)) &= -\sqrt{2} g' \sqrt{m_{\mu_1}^2 - m_{B_1}^2} \times \\
&\quad e^{+i\phi_1/2} \sin\frac{\theta_1}{2} \\
\mathcal{M}(\mu_{1R}^-(\downarrow) \to \mu_R^- B_1(-1)) &= 0 \\
\mathcal{M}(\mu_{1R}^-(\downarrow) \to \mu_R^- B_1(0)) &= g' \frac{m_{\mu_1}}{m_{B_1}} \sqrt{m_{\mu_1}^2 - m_{B_1}^2} \times \\
&\quad e^{-i\phi_1/2} \sin\frac{\theta_1}{2} \\
\mathcal{M}(\mu_{1R}^-(\downarrow) \to \mu_R^- B_1(+1)) &= \sqrt{2} g' \sqrt{m_{\mu_1}^2 - m_{B_1}^2} \times \\
&\quad e^{-i\phi_1/2} \cos\frac{\theta_1}{2}.
\end{aligned} \tag{3.22}$$

We see here the dependence on the helicity of the μ_{1R} as in Eq. (3.5). Similar equations hold for the decay of μ_{1R}^+, with $\phi_1 \to \phi_2$ and $\theta_1 \to \theta_2$.

The total cross section for the event is the coherent sum over μ_{1R} helicities and the incoherent sum over the helicities h of the electrons and polarizations λ of the KK photons:

$$\begin{aligned}
d\sigma &= \frac{d\Phi_4}{4} \sum_{L,R,\lambda\lambda'} \left| \sum_{hh'} \mathcal{M}(e_{L/R}^- e_{R/L}^+ \to \mu_{1R}^-(h)\mu_{1R}^+(h')) \right. \\
&\quad \left. \mathcal{M}(\mu_{1R}^-(h) \to \mu_R^- B_1(\lambda)) \mathcal{M}(\mu_{1R}^+(h') \to \mu_R^+ B_1(\lambda')) \right|^2 \\
&\quad 2\pi\delta(s_{\mu^+ B_1} - m_{\mu_1}^2) 2\pi\delta(s_{\mu^+ B_1} - m_{\mu_1}^2) \frac{1}{(2m_{\mu_1}\Gamma)^2}.
\end{aligned} \tag{3.23}$$

Once again, Γ is the total width of μ_{1R} and there is an implied momentum-conserving δ function.

Chapter 4

KK Gravitons at the LHC

The Large Hadron Collider (LHC) at CERN is expected to produce a wealth of discoveries by probing the TeV scale for the first time. Apart from finally accessing the electroweak symmetry breaking scale and thus potentially discovering the elusive Higgs boson, we expect to see new physics that resolves the hierarchy/naturalness problem [6, 7, 8, 9] and perhaps provides an insight into the nature of dark matter. One exciting possible solution to the hierarchy problem is the existence of warped extra dimensions [16, 17] which allows for TeV scale gravitational interactions. There are many variations of the basic theory [50], but one common feature that they share is the existence of heavy Kaluza-Klein (KK) gravitons.

For the purpose of this chaper we will consider a Randall-Sundrum model with 3+1 dimensional spacetime with one additional warped extra dimension (RS1). The SM fields are confined to a 3+1 dimensional TeV brane and the graviton propagates freely in the 4+1 dimensional bulk. Quantization of the graviton wave function in the extra dimension, with boundaries between the TeV brane and a Planck brane, leads to various modes which appear as heavy spin-2 fields in the 3+1 dimensional effective theory on the TeV brane.

One of the challenges at the LHC will be to determine the spins of newly discovered particles in order to distinguish various theoretical models. The KK graviton provides a unique signature of gravitational physics at the TeV scale by virtue of its spin-2 nature. Thus, it becomes crucial to have techniques to identify its spin. So far, the technique proposed to measure KK graviton spin at the LHC relies on resonant graviton production followed by decay into a lepton pair [51, 52, 53, 54, 55]. By looking at the polar angular dependence of the leptons relative to the beam axis, one sees a quartic behavior of the differential cross section,

$$\frac{d\sigma}{d\cos\theta} = A\cos^4\theta + B\cos^2\theta + C. \tag{4.1}$$

Recently, a new technique for measuring spin has been proposed. One can look at quantum interference of helicity states in the azimuthal angular dependence of particle decays to study their spin in a model-independent way [32, 1]. The goal of this chapter is to apply this technique to study the KK graviton spin and look at its feasibility at the LHC.

4.1 Model Parameters

The interaction between the massive KK gravitons and the SM fields in the 4-d effective theory is given by the Lagrangian [57, 58],

$$\mathcal{L}_{int} = -\frac{1}{\Lambda}\sum_{n} G^{(n)\mu\nu}\mathcal{T}_{\mu\nu}. \tag{4.2}$$

Here, $G^{(n)\mu\nu}$ represents the nth KK graviton mode, and $\mathcal{T}_{\mu\nu}$ is the stress-energy tensor of the SM Lagrangian given by

$$\mathcal{T}_{\mu\nu} = -\eta_{\mu\nu}\mathcal{L}_{SM} + 2\frac{\delta\mathcal{L}_{SM}}{\delta g_{\mu\nu}}\bigg|_{g_{\mu\nu}=\eta_{\mu\nu}}. \tag{4.3}$$

Λ is the coupling, given by

$$\Lambda = e^{-kr_c\pi}\bar{M}_{pl}, \tag{4.4}$$

where k is of the order of the Planck scale, r_c is the compactification radius of the extra dimension and $\bar{M}_{pl} \equiv M_{pl}/\sqrt{8\pi}$ is the reduced Planck scale. Note the absence of KK-parity which allows the heavy graviton modes to decay into purely SM particles.

The mass of the nth KK-graviton is given by,

$$m_n = x_n\Lambda\frac{k}{\bar{M}_{pl}}, \tag{4.5}$$

where x_n are the nth zeros of the J_1 Bessel function. While studying the properties of the n = 1 KK graviton we can thus regard this theory as being dependent on only two parameters, Λ and k, or equivalently the dimensionless coupling $c \equiv \frac{k}{\bar{M}_{pl}}$ and m_1, the mass of the KK graviton of interest.

Naturalness constraints require Λ to be less than about 10 TeV. In order for an effective field theory description of gravity to be valid we require that the 5-d curvature bound, $|R_5| < M_5^2$, is satisfied, where M_5 is the 5-d Planck scale. By looking at the various theoretical and experimental constraints on the model parameters [52] (Figure 4.1), we expect c to lie roughly between 0.01 (weakly coupled) and 0.1 (strongly coupled). We consider m_1 in the range of 750 GeV - 2 TeV. The decay width of the graviton to SM particles can be evaluated by using the expressions given in [58, 53, 59]. In the limit that decay particle masses can be neglected, the decay width of the graviton is given by

$$\Gamma_n = \alpha m_n (x_n c)^2, \tag{4.6}$$

where α is a constant depending upon the number of open decay channels. If one assumes decay to only SM particles, the ratio $\Gamma_1 : m_1$ is found to be 1.37% for $c = 0.1$ (assuming a Higgs mass of 120 GeV and decay into SM particles only). This value is in disagreement with the value 1.43% cited in the literature [60].

4.2 Using Azimuthal Angular Dependence to Measure Spin

To determine the spin of a particle X, we consider the production process $A + B \to X + Y$, where X further decays to $M + N$. Here, A and B refer to beam particles or partons, and X is the parent particle whose spin we wish to measure. M and N are the daughter particles that X decays into.

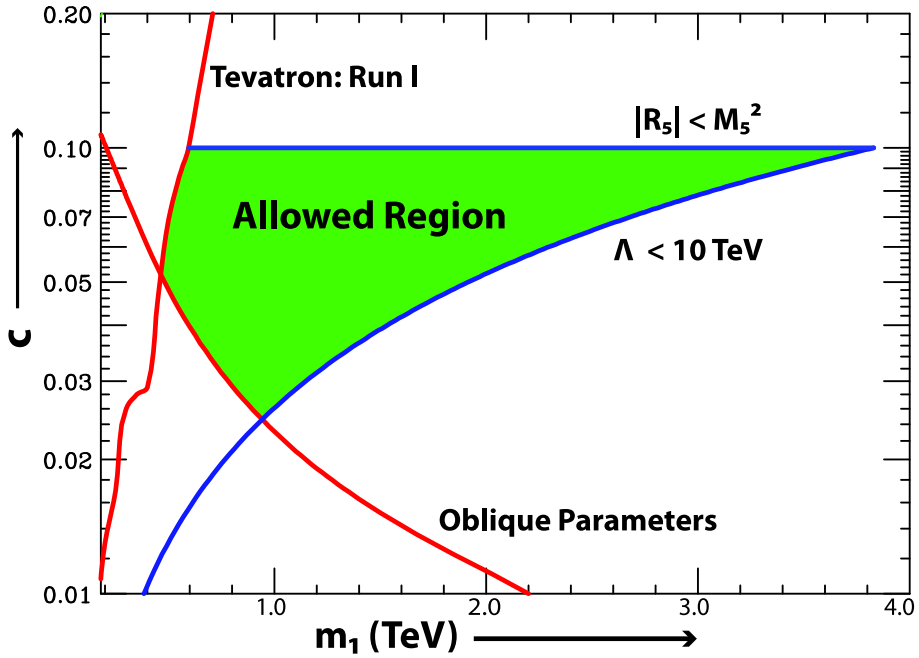

Figure 4.1: Experimental and theoretical constraints on the KK graviton parameters in the $c - m_1$ plane. Red curves show experimental constraints and blue curves show theoretical constraints. The green shaded region shows the allowed parameter space.

This gives us two planes to consider, namely the production plane (defined by the beam direction and the parent momentum) and the decay plane (defined by the parent momentum and either daughter) (Figure 4.2).

Now consider the daughter M with momentum $\vec{p}_M$. The angle it makes with the parent momentum $\vec{p}_X$ is defined to be θ. Projecting out the component of $\vec{p}_M$ parallel to $\vec{p}_X$ and looking at the angle between the residual vector and the production plane we define an angle ϕ. Thus, ϕ describes azimuthal rotations of the vector $\vec{p}_M$ in the $x - y$ plane with $\vec{p}_X$ taken to be the z-axis. From the figure it is clear that, equivalently ϕ can be defined as the angle between the production plane and the decay plane. More explicitly, we define the two vectors,

$$\vec{p}_{prod} = \vec{p}_A \times \vec{p}_X \tag{4.7}$$

and

$$\vec{p}_{decay} = \vec{p}_X \times \vec{p}_M. \tag{4.8}$$

Then

$$\cos\phi = \hat{p}_{prod} \times \hat{p}_{decay}, \tag{4.9}$$

where $\hat{p}$ denotes the normalized vectors.

In the limit of the narrow-width approximation, the amplitude can be split into $\mathcal{M}_{prod}$ and $\mathcal{M}_{decay}$,

$$\mathcal{M}_{prod} = \langle X, Y | \mathcal{T}_{prod} | A, B \rangle \tag{4.10}$$

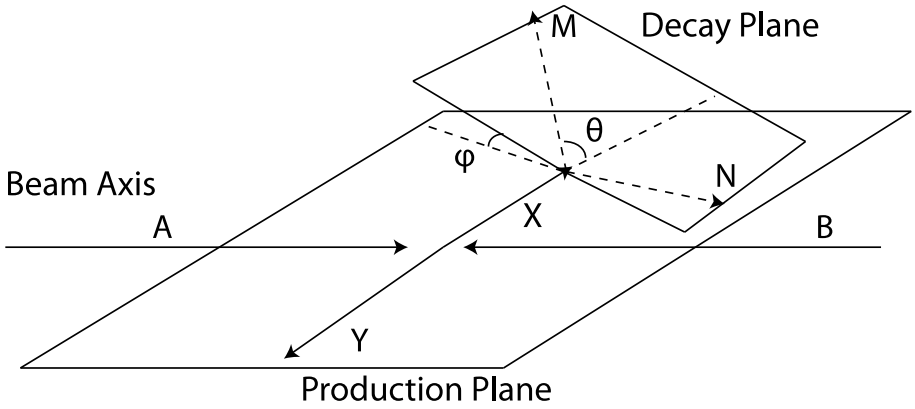

Figure 4.2: Production and decay planes of the process $A + B \to X + Y \to M + N$. The angle ϕ is defined as the azimuthal angle between $\vec{p}_X$ and $\vec{p}_M$, or equivalently the angle between the production and decay planes.

$$\mathcal{M}_{decay}(\phi) = \langle M, N, \phi | \mathcal{T}_{decay} | X \rangle, \tag{4.11}$$

where we have explicitly shown the ϕ dependence of the the final state and decay amplitude. We also have

$$\mathcal{M}_{decay}(\phi) = \langle M, N(\phi = 0) | e^{+iJ_z\phi} \mathcal{T}_{decay} | X \rangle, \tag{4.12}$$

where J_z generates rotations about the $\vec{p}_X$ direction. We can now think of the rotation operator as acting on the interaction $\mathcal{T}$-matrix plus ket, rather than on the bra. Assuming $\mathcal{T}_{decay}$ is rotationally invariant, we only need to consider rotations of the particle X about its own momentum axis. In this case,

$$J_z = \vec{J} \cdot \hat{p} = (\vec{s} + \vec{r} \times \vec{p}) \cdot \hat{p} = \vec{s} \cdot \hat{p} = h. \tag{4.13}$$

Thus, rotations about the momentum axis of a given helicity state, h for X only produce a phase $e^{+ih\phi}$. So,

$$\mathcal{M}_{decay}(\phi) = e^{+ih\phi} \mathcal{M}_{decay}(\phi = 0). \tag{4.14}$$

Thus, allowing for production over all possible helicity states of X we must sum coherently over all possible amplitudes, and the differential cross section takes the form

$$\frac{d\sigma}{d\phi} \propto \left| \sum_h \mathcal{M}_{prod} e^{+ih\phi} \mathcal{M}_{decay}(\phi = 0), \right|^2 \tag{4.15}$$

where h runs from $-s$ to $+s$ and X has spin s. From this it is clear that, if we look at the differential distribution $d\sigma/d\phi$, interference between various helicity states is responsible for a non-trivial ϕ dependence,

$$\frac{d\sigma}{d\phi} = A_0 + A_1 \cos(\phi) + A_2 \cos(2\phi) + ... + A_{2s} \cos(2s\phi). \tag{4.16}$$

Note the absence of $\sin(n\phi)$ modes, which would be present in the case of CP violating processes.

The SM has no particles with spin greater than 1 and so the largest mode from the SM would only be $\cos(2\phi)$, corresponding to X being a gauge boson. We can now see the unique signature that the KK graviton will produce, namely a $\cos(4\phi)$ mode.

Also, we note that this result is valid in any reference frame, but the size of the coefficients A_i will be different in different reference frames. To maximize this unique signature for the KK graviton, we need to choose a reference frame in which A_4/A_0 has a large value.

4.3 Signal and Background

We assume that the mass of the graviton will be well measured using resonant graviton production through the process $pp \to G \to l^+l^-$ [51, 52].

The process we are considering is $pp \to G$ + jet followed by $G \to l^+\ l^-$, where l are muons or electrons. The dominant parton level subprocess comes from $gg \to Gg$ with subdominant $q(\bar{q})\ g \to G\ q(\bar{q})$ and the crossed channel $q\ \bar{q} \to G\ g$. Here G represents the graviton, g represents gluons, and q represents the various quarks.

The SM background comes from the subdominant channels with G replaced by an off-shell Z, γ. This is the exact analog of Drell-Yan background in resonant graviton production. Cutting on the invariant mass of the lepton pair in a mass window around the graviton mass gets rid of most of the background. The SM background consists of spin-1 states and can not give any contribution to A_4. At most it can affect the value of A_0 and dilute the value of A_4/A_0.

4.4 Calculating the Differential Cross Section

4.4.1 Zero Rapidity Frame

The dilepton + jet events that we are looking for are fully reconstructible at the LHC. The key reason for this is that we have a signature with no missing energy-momentum which in turn is a direct consequence of the absence of KK parity. The graviton 4-momenta should have minor errors compared to the jet reconstruction since it is reconstructed from the dilepton 4-momenta. As previously mentioned, the size of the nonzero coefficients A_i are frame dependent, and so we must choose a frame in which the normalized coefficient $S_4 \equiv |A_4/A_0|$ is large. It was found that in the center-of-mass frame of the partonic processes, S_4 was larger than in the lab frame. However, transforming from the lab frame to the center-of-mass frame would have an error dependent on the error of the jet reconstruction. To avoid this error and still make an improvement in the signal, we studied S_4 in the zero-rapidity frame of the graviton, i.e., the frame where the graviton is purely transverse to the beam axis (Figure 4.3). The reason for this is that the boost factor can be calculated from just the graviton momentum in the lab frame, which is well reconstructed from the leptons.

4.4.2 Cuts

The first set of cuts used included a pseudo-rapidity ($|\eta| < 2.5$) cut and a $p_T > 20$ GeV cut for the jet. The second set of cuts was a mass-window cut on the invariant mass distribution of the lepton pair. This gets rid of a large portion of the SM background. The size of the window was determined by detector resolution at ATLAS [63, 64] for an e^+e^- pair. The third set of cuts involved rapidity cuts

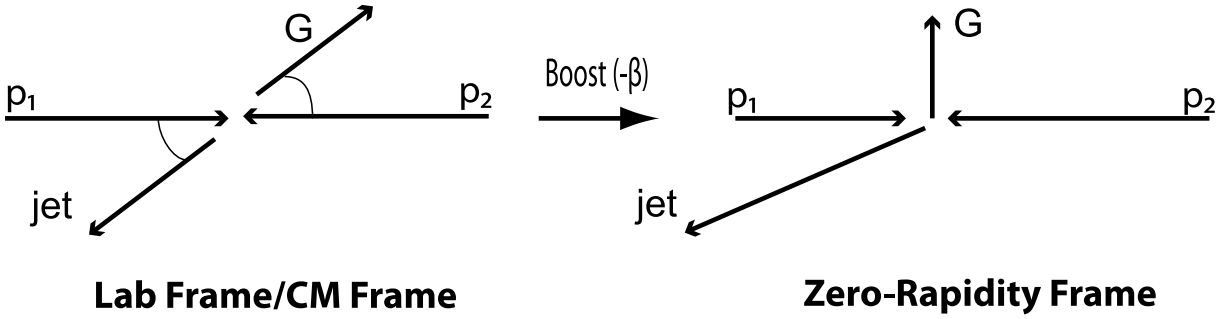

Figure 4.3: Boost from the center-of-mass or laboratory frame to the zero-rapidity frame

($|\eta| < 2.6$) on each of the leptons with a requirement that $p_T > 10$ GeV for either one of the leptons and $p_T > 20$ GeV for the other. An isolation cut, $\Delta r \equiv \sqrt{(\Delta\eta)^2 + \Delta\phi^2} > 0.7$, was imposed between the lepton and the jet. However, the third set of cuts affects the angular distribution of the leptons and can create false cosine modes in the differential distribution.

To solve this problem one imposes "rotationally invariant cuts," first introduced in [56]. Thus, it is not sufficient for the observed lepton to simply pass these cuts; the leptons are rotated around the graviton momentum axis in small increments and at each step it is checked that the lepton passes the cuts. The added complication is that the rotations must be made in the zero-rapidity frame to preserve rotational invariance in that frame (Figure 4.4). So, the procedure is as follows:

1. First, reconstruct the event completely using the dilepton and jet signals.
2. Calculate the boost factor to take us from the lab frame to the zero-rapidity frame of the graviton.
3. Boost all momenta to the zero-rapidity frame. Rotate the leptons about the graviton momentum direction by a small angle, say 1°.
4. Reboost the new lepton and jet momenta to the lab frame. Check if they pass the cuts; if they don't, throw out the event.
5. If they do pass the cuts go back to step 3.
6. Repeat this procedure until we have made a full 360° rotation of the lepton momenta about the graviton momentum axis in the zero-rapidity frame.

This procedure ensures that the cuts do not affect the azimuthal angular distribution in the zero-rapidity frame.

4.4.3 Simulations

We used HELAS [34] with spin-2 particles [65] to calculate the helicity amplitudes for the graviton scattering process. LHApdf [66] was used to fold in the parton distribution functions for the protons. We used the pdf set CTEQ6L [78]. An adaptive Monte-Carlo package, BASES [35], was used to perform the integration over phase space and produce the differential cross section $d\sigma/d\phi$.

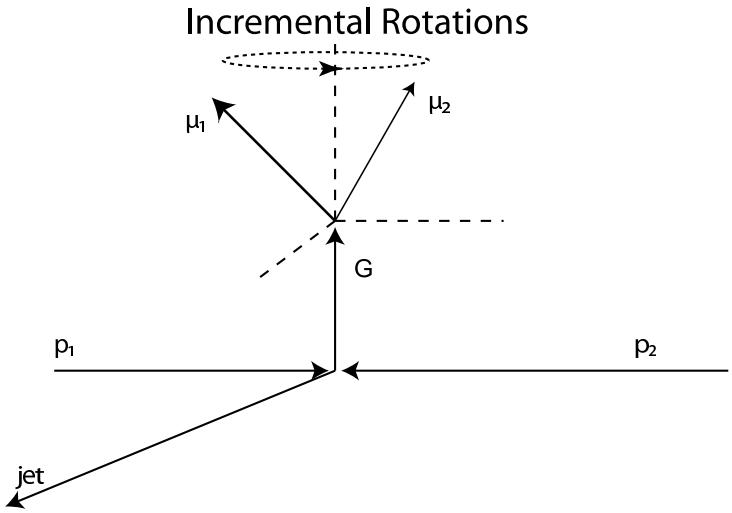

Figure 4.4: The leptons are rotated about the graviton momentum axis in the zero rapidity frame. The dilepton + jet momenta must be reboosted to the lab frame at each step to make sure that they pass the cuts.

4.5 Determining the Coefficients of the Various Cosine Modes

Once we have the binned distribution $d\sigma/d\phi$ with $2n$ bins (For the purposes of calculation in this chapter we used 50 bins), we try to fit coefficients of the form

$$\begin{aligned} x_i &\equiv \frac{1}{\text{Binsize}} \int_{\frac{2\pi(i-1)}{2n}}^{\frac{2\pi i}{2n}} \frac{d\sigma}{d\phi} d\phi \\ &= \frac{1}{2\pi/2n} \int_{\frac{2\pi(i-1)}{2n}}^{\frac{2\pi i}{2n}} \left[\sum_{j=0}^{n-1} A_j \cos(j\phi) \right. \\ &\qquad \left. + \sum_{j=1}^{n} B_j \sin(j\phi) \right] d\phi, \end{aligned} \tag{4.17}$$

where i runs over 0, 1, 2, ..., $2n-1$. The integration accounts for the binning process and the $2n$ coefficients A_0, ..., A_{n-1}, B_1, ..., B_n correspond to the strengths of the various cosine and sine modes that can be resolved from each other.

Thus, we have a simple linear relationship between the $2n$ binned values of $d\sigma/d\phi$ (x_i) and the $2n$ binned-Fourier coefficients (y_j) of the form $x_i = p_{ij} y_j$. Here, p_{ij} are either of the form $\int_{\frac{2\pi(i-1)}{2n}}^{\frac{2\pi i}{2n}} \cos(j\phi) d\phi$ or $\int_{\frac{2\pi(i-1)}{2n}}^{\frac{2\pi i}{2n}} \sin(j\phi) d\phi$.

Now, we can simply invert this matrix for a given value of n to recover the amplitudes of the various harmonics. For the $d\sigma/d\phi$ distribution for the graviton we expect to see only the coefficients A_0, ..., A_4 to be nonzero. Also, since the beams are identical, we expect to see only the even cosine modes. The odd cosine modes drop out since they flip sign when the beams are switched ($\phi \to \pi - \phi$).

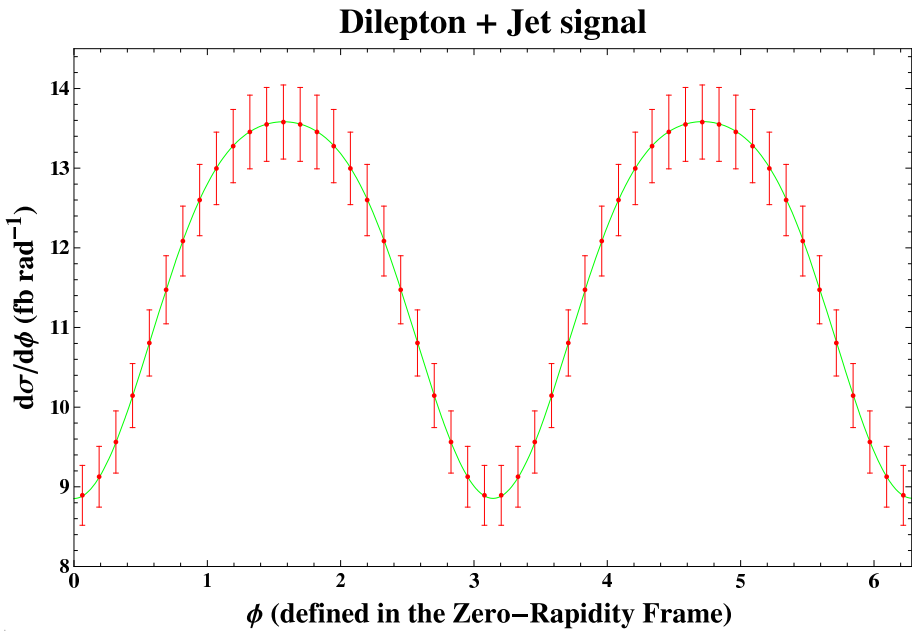

Figure 4.5: Differential distribution ($\frac{d\sigma}{d\phi}$) for m_1 = 1 TeV and c = 0.05. A strong $\cos(2\phi)$ mode can be seen but there is also a $\cos(4\phi)$ component. The theoretical curve (produced from simulations) is shown in green. The red dots indicate the binned values, with error bars corresponding to Gaussian errors for a luminosity of 500 fb^{-1}.

4.6 Results and Discussion

Simulations were done for the process $pp \to e^+e^-j$ at 7 TeV beam energy using a dilepton invariant mass window cut around the graviton mass. Figure 4.5 shows the $d\sigma/d\phi$ distribution for a 1 TeV graviton with $c = 0.05$. Figure 4.6 shows the normalized fitted coefficients. The normalized cosine coefficients (S_i) are shown in the first 25 bins, with the zero mode suppressed. The next 25 bins show the sine modes. The size of the S_4 coefficient is 3.14%. Note the absence of odd cosine modes; this arises from the fact that we are using identical beams.

To look at the dependence of the signal on graviton mass, simulations were performed for $c = 0.1$ and m_1 = 750 GeV, 1 TeV, 1.5 TeV, and 2 TeV. The results are summarized in Table 4.1. The

m_1 (TeV)	Δm (GeV)	σ_{total} (fb)	σ_{bgd} (fb)	S_2	S_4
0.75	24.4	871.7	0.39	20.00%	3.50%
1.0	30.7	229.8	0.15	20.48%	3.16%
1.5	42.8	28.7	0.03	20.70%	1.52%
2.0	55.0	5.52	0.01	20.08%	0.80%

Table 4.1: Signal strength $S_4 \equiv |A_4/A_0|$ as a function of the mass of the graviton. c = 0.1 for all entries. S_2 is shown for comparison. The mass window (based on the ATLAS detector resolution for e^+e^- invariant mass [63, 64]) cuts out most of the background.

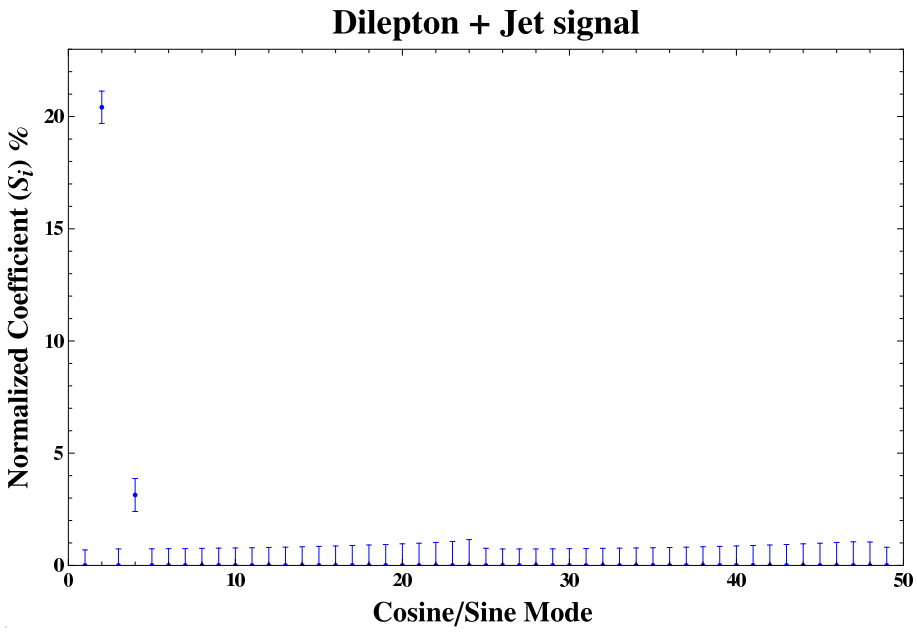

Figure 4.6: Fitted cosine coefficients of the binned differential cross section shown in Figure 4.5 corresponding to 50 bins. The first 25 modes label the normalized cosine modes, the next 25 show the sine modes. (The large 0-mode which would be 100% is not shown.) See text for how the error bars in this plot are calculated using error bars from the binned differential cross section.

total cross section decreases rapidly with graviton mass, as expected. The background is negligible and, as we will see in the next paragraph, has little effect even if the coupling c is reduced. The main concern is therefore the decrease in S_4 and the low cross section at large values of m_1.

The results for a 1 TeV graviton at different values of the coupling c are shown in Table 4.2. In the absence of cuts the graviton cross section is expected to approximately scale like c^2. The SM background level is 0.15 fb which is $\sim 5\%$ at $c = 0.01$. The value of S_4 is expected to be diluted slightly by the background because of a corresponding 5% increase in A_0. As c is increased, the background as a percentage of the cross section decreases and S_4 is restored to its maximum strength.

c	σ_{total} (fb)	S_2	S_4
0.01	3.27	18.62%	3.05%
0.02	12.51	20.02%	3.15%
0.05	72.75	20.42%	3.14%
0.1	229.8	20.48%	3.16%

Table 4.2: Signal strength $S_4 \equiv |A_4/A_0|$ as a function of the coupling c. All entries are for m_1 = 1 TeV. S_2 is shown for comparison. The SM background cross section is 0.15 fb.

4.7 Error Analysis

As we have seen, the effect of background is small and does not contribute to A_4. Its only effect is to dilute the normalized coefficient S_4. Thus, the experimental error will be determined by event statistics. We assumed Gaussian errors ($\Delta x_j = x_j \frac{\sqrt{N_j}}{N_j}$) in the jth bin assuming $N_j = \mathcal{L}\sigma \frac{x_j}{\sum x_j}$ events in each bin for integrated luminosities $\mathcal{L}$ of 10, 100, and 500 fb^{-1}. Since the coefficients A_i are determined from the binned values x_j through a simple linear relationship (via the matrix $q_{ij} = p_{ij}^{-1}$), it is then straightforward to work out the errors in the normalized coefficients (ΔS_i):

$$\Delta S_i = \sqrt{\sum_j \left(\frac{q_{ij}}{A_0} - \frac{S_i}{A_0} q_{0j} \right)^2 \Delta x_j^2}. \tag{4.18}$$

The first term in the parentheses arises from the simple linear relationship between A_i and x_j. The second term comes from the error associated with the normalization factor A_0. The relative errors ($\frac{\Delta S_4}{S_4}$) for various integrated luminosities at different points in the parameter space of the model are given in Table 4.3. A value > 1 for the relative error indicates that statistics would be poor and gives no reason to doubt S_4 being consistent with 0. A value of 0.20 or less indicates at least a 5σ effect, indicating high likelihood of confirmation of the spin-2 nature of the KK graviton.

m_1 (TeV)	c	10 fb^{-1}	100 fb^{-1}	500 fb^{-1}
0.75	0.1	0.43	0.14	0.06
1.0	0.01	8.03	2.54	1.14
1.0	0.02	3.97	1.26	0.56
1.0	0.05	1.65	0.52	0.23
1.0	0.1	0.93	0.29	0.13
1.5	0.1	5.42	1.71	0.77
2.0	0.1	23.52	7.44	3.32

Table 4.3: Statistical error $\Delta S_4/S_4$ for different integrated luminosities for the process $pp \to e^+e^-j$. $\Delta S_4/S_4 < 0.5(0.71)$ corresponds to a 2σ confirmation of the graviton spin, and $\Delta S_4/S_4 < 0.2(0.28)$ corresponds to a 5σ confirmation. The values in brackets denote the 2σ and 5σ confidence levels if one includes $\mu^+\mu^-j$ production channels as well.

Alternatively, if one requires only a 95% confidence level (2σ) effect, then a value of 0.5 or less for $\Delta S_4/S_4$ should suffice. If we assume information from $\mu^+\mu^-j$ statistics in addition to the e^+e^-j channel (assuming that detector resolution for the invariant mass is the same for both lepton species), then we can see a factor 2 improvement in the statistics. This would in turn result in a factor $\sqrt{2}$ drop in the error. Thus, in this case the parameter space in Table 4.3 for which $\Delta S_4/S_4 < 0.71$ would correspond to potential for a 2σ confirmation of the graviton spin, and $\Delta S_4/S_4 < 0.28$ would correspond to a 5σ confirmation.

4.8 Comparison with Resonant Graviton Production Method and Distinction from Spin-0

Osland et al. [54, 55] consider the resonant graviton production process $pp \to G \to l^+l^-$ to measure the spin of the graviton using the quartic angular dependence of the polar angle of the lepton. This results in a center-edge asymmetry (A_{CE}) in the differential distribution $d\sigma/d\cos\theta$. Their results indicate (2σ) identification of the graviton spin for $c = 0.01$ and 10^{-1} fb of luminosity for masses up to 1.1 TeV. For $c = 0.1$ they claim identification up to masses of 2.4 TeV.

The azimuthal angular dependence method that we considered has inherently lower statistics compared to resonant graviton production because of the extra recoiling jet. Our method suffers from lower statistics, but given higher luminosities, it can still provide an independent confirmation of the KK graviton spin for a large region of the expected parameter space of the KK graviton.

The center-edge asymmetry method can distinguish a spin-1 particle (Z') from a KK graviton more readily than it can distinguish it from a spin-0 particle.

Our method proves complementary, since the KK graviton also produces a large $\cos(2\phi)$ mode ($S_2 \approx 20\%$) and can thus easily be distinguished from a scalar which would not produce any nonzero modes. The results for $\Delta S_2/S_2$ are shown in Table 4.4.

m_1 (TeV)	c	10 fb^{-1}	100 fb^{-1}	500 fb^{-1}
0.75	0.1	0.07	0.02	0.01
1.0	0.01	1.30	0.41	0.18
1.0	0.02	0.62	0.19	0.09
1.0	0.05	0.25	0.08	0.04
1.0	0.1	0.14	0.04	0.02
1.5	0.1	0.39	0.12	0.06
2.0	0.1	0.93	0.29	0.13

Table 4.4: Statistical error $\Delta S_2/S_2$ for different integrated luminosities for the process $pp \to e^+e^-j$. $\Delta S_2/S_2 < 0.5(0.71)$ corresponds to a 2σ distinction from a spin-0 particle, and $\Delta S_2/S_2 < 0.2(0.28)$ corresponds to a 5σ distinction. The values in brackets denote the 2σ and 5σ confidence levels if one includes $\mu^+\mu^-j$ production channels as well.

Assuming, as before, inclusion of $\mu^+\mu^-$ statistics, $\Delta S_2/S_2 < 0.71$ corresponds to a 2σ distinction from a spin-0 particle, and $\Delta S_2/S_2 < 0.28$ corresponds to a 5σ distinction. In regions of the parameter space of m_1, where the SM background is comparable to the cross section of interest (Table 4.1), the confidence levels are altered slightly because the off-shell γ and Z, being spin-1, contribute to the A_2 coefficient.

From the table, we can see that even with 10 fb^{-1} of luminosity, the spin-0 hypothesis can be ruled out for a large portion of the allowed parameter space. Thus, our method proves complementary to the approach by Osland et al. by ruling out spin-0 more easily than spin-1. In both methods the distinction from spin-0 can be made from comparable integrated luminosities.

4.9 Summary and Conclusion

We studied the process $pp \to G$ jet $\to l^+l^-$ jet and looked at the differential distribution $d\sigma/d\phi$. The distribution was found to have a $\cos(4\phi)$ mode, characteristic of a spin-2 particle, with strength parametrized by S_4. The parameter S_4 was $\sim 3\%$ for values of m_1 below a TeV. As we go to higher graviton masses the signal drops off, but what is of more concern is the drop in cross cross section with large m_1 or low values of c. Both of these scenarios are unlikely to occur in conjunction of naturalness constraints (see Figure 4.1).

In conclusion, observing higher cosine modes (> 2) in the differential distribution would be a clear signal of physics beyond the Standard Model. Observing the $\cos(4\phi)$ mode at the LHC would be a strong indicator of gravitational physics at the TeV scale. If the coupling is strong enough, ~ 0.05 or greater, and the mass is sufficiently low, ~ 1 TeV or less, we expect to have a clear signal of the spin-2 nature of the KK graviton at the LHC.

For regions of parameter space with larger masses or lower couplings, the azimuthal angular dependence of the cross section is still useful in ruling out the spin-0 hypothesis and this can be done for fairly low luminosities (~ 10 fb^{-1}) as well.

This method provides an important complementary and independent approach to measuring the spin of the KK graviton, as compared to the method of using polar angular dependence from resonant KK-graviton production.

Chapter 5

Sextet

The Large Hadron Collider (LHC) at CERN will soon provide a great opportunity for exploring physics at the TeV scale. As a proton-proton collider with a total center-of-mass energy of 14 TeV, the LHC is truly a Quantum Chromodynamics (QCD) machine. We therefore wish to study color exotics, since any accessible new physics in the strong interaction sector will appear in the early stages of LHC operation. Many models of physics beyond the SM naturally require the presence of color exotics, such as gluinos and squarks in supersymmetric extensions of the SM, KK-gluons and KK-quarks in extra dimensional models, or the top-prime in Little Higgs or twin Higgs models. All of these are either quark or gluon partners which belong (respectively) to the fundamental and adjoint representations of the QCD gauge group $SU(3)_C$ respectively. It is natural to consider colored particles in other representations; in this chapter, we focus on a scalar which is in the sextet(6) representation of $SU(3)_C$. Color sextet particles have been widely discussed in nuclear physics as diquark condensate states; in the SSC era, sextet quarks were discussed in [68].

Color sextet scalars are naturally present in partial unification [69], grand unification [70], and composite models; in some cases they may be present around the weak scale. For instance, in a supersymmetric Pati-Salam $SU(2)_R \times SU(2)_L \times SU(4)_C$ model, light color sextet scalars can be realized around the weak scale, even though the scale of $SU(2)_R \times SU(4)_C$ symmetry breaking is around 10^{10} GeV due to the existence of accidental symmetries, with the masses of color sextet Higgs arising only through high-dimension operators [71, 72]. In this case, the introduction of a color sextet Higgs will not lead to proton decay but only to neutron-antineutron ($n - \bar{n}$) oscillation, and is fully compatible with present limits [71, 72]. In a similar framework, light color sextet scalars also help in post-sphaleron baryogenesis [74]. In this chapter, however, we will take a purely phenomenological approach toward the sextet scalar without assuming any model a priori.

Among all the color exotics, the color sextet scalar is unique in its coupling to quarks. In group theory language, the color sextet lies in $3 \otimes 3 = 6 \oplus \bar{3}$ as a symmetric second rank tensor under $SU(3)_C$. The Lorentz structure for this scalar coupling to quarks is given by $\psi^T C^{-1} \psi \phi$, where ψ is a Dirac spinor and ϕ is the scalar. Under the SM gauge group $SU(3)_C \times SU(2)_L \times U(1)_Y$, the sextet scalar can be Δ_6, a $SU(2)_L$ adjoint $(6, 3, 1/3)$; Φ_6, a $SU(2)_L$ singlet $(6, 1, 4/3)$; ϕ_6, a $SU(2)_L$ singlet $(6, 1, -2/3)$; or δ_6, a $SU(2)_L$ singlet $(6, 1, +1/3)$. The color sextet scalars are also charged under the global baryon symmetry $U(1)_B$ and the electromagnetic symmetry $U(1)_{\rm EM}$. To avoid breaking $U(1)_{\rm EM}$, these scalar fields should not develop a nonzero vacuum expectation value. This condition removes any possibility of $n - \bar{n}$ oscillation in the minimal model involving color sextet scalars. We may write down the flavor-

independent Lagrangian of such a minimal model by only considering SM gauge invariants and keeping $U(1)_{\rm EM}$ unbroken,

$$\begin{aligned}
\mathcal{L} &= \mathrm{Tr}[(D_\mu\Delta_6)^\dagger(D^\mu\Delta_6)] - M_\Delta^2\mathrm{Tr}[\Delta_6^\dagger\Delta_6] + f_\Delta Q_L^T C^{-1}\tau_2\Delta_6^\dagger Q_L \\
&+ (D_\mu\Phi_6)^\dagger(D^\mu\Phi_6) - M_\Phi^2\Phi_6^\dagger\Phi_6 + f_\Phi u_R^T C^{-1} u_R\Phi_6^\dagger \\
&+ (D_\mu\phi_6)^\dagger(D^\mu\phi_6) - M_\phi^2{\phi_6}^\dagger\phi_6 + f_\phi d_R^T C^{-1} d_R\phi_6^\dagger \\
&+ (D_\mu\delta_6)^\dagger(D^\mu\delta_6) - M_{\delta_6}^2{\delta_6}^\dagger\delta_6 + f_\delta d_R^T C^{-1} u_R\delta_6^\dagger \\
&- \lambda_\Delta(\mathrm{Tr}[\Delta_6^\dagger\Delta_6])^2 - \lambda_\Phi(\Phi_6^\dagger\Phi_6)^2 - \lambda_\phi({\phi_6}^\dagger\phi_6)^2 - \lambda_\delta({\delta_6}^\dagger\delta_6)^2 \\
&- \lambda'_\Delta\mathrm{Tr}[\Delta_6^\dagger\Delta_6\Delta_6^\dagger\Delta_6] - \mathrm{Tr}[\Delta_6^\dagger\Delta_6](\lambda_1{\Phi_6}^\dagger\Phi_6 + \lambda_2{\phi_6}^\dagger\phi_6 + \lambda_3{\delta_6}^\dagger\delta_6) \\
&- \lambda_4{\Phi_6}^\dagger\Phi_6{\phi_6}^\dagger\phi_6 - \lambda_5{\Phi_6}^\dagger\Phi_6{\delta_6}^\dagger\delta_6 - \lambda_6{\phi_6}^\dagger\phi_6{\delta_6}^\dagger\delta_6\ , \qquad (5.1)
\end{aligned}$$

where the QCD covariant derivative is defined as $D_\mu = \partial_\mu - ig_s G_\mu^a T_r^a$, and the T_r^a are the representation matrices for the sextet; M_i^2, λ_i, and f_i are all positive-definite model parameters.

If we consider the $SU(2)_L$ adjoint sextet scalar Δ_6, there will be three physical sextet scalar states that couple to up-type quark pairs, down-type quark pairs, and up-down-type quark pairs. When the sextet scalar decays into light quark states, the existing search strategies for massive octet scalars or vectors [75] may be employed. Δ_6, Φ_6, and δ_6 may all contribute to the single top plus jet signal and $t\bar{t}+Nj$ signal from pair production. Here we consider the scenario in which a color sextet scalar decays into a top-quark pair so that one can use the leptons from the top quark decay to determine the features of the sextet. The signature that contains multi-top final states has been discussed in the context of many new physics models as resonance decaying into top quarks or top composite[72, 73]. To illustrate this and simplify our search, our study will focus on the color sextet $SU(2)$ singlet scalar Φ_6 that only couples to right-handed up-type quarks.

5.1 Decay of the Color Sextet Scalar

The decay of the Φ_6 depends on its mass, M_{Φ_6}, and its couplings to quarks, f_{ij} $(i,j = u,c,t)$. To illustrate our reconstruction algorithm in the discussion of discovery, we consider the case where $M_{\Phi_6} > 350$ GeV and the Φ_6 decays into two onshell top quarks; other mass ranges are discussed in the conclusion section. Above threshold, the general expression for the decay partial widths of the sextet scalar are

$$\begin{aligned}
\Gamma_{ii} &= \frac{3}{16\pi}|f_{ii}|^2 M_{\Phi_6}\lambda^{1/2}(1, r_i^2, r_i^2)(1-4r_i^2) \\
\Gamma_{ij} &= \frac{3}{8\pi}|f_{ij}|^2 M_{\Phi_6}\lambda^{1/2}(1, r_i^2, r_j^2)(1-r_i^2-r_j^2), \qquad (5.2)
\end{aligned}$$

where $\lambda(x,y,z) = (x-y-z)^2 - 4yz$ and $r_i = m_i/M_{\Phi_6}$.

By far, the most stringent bounds on these parameters come from $D^0 - \bar{D}^0$ mixing, to which Φ_6 would make a tree-level contribution proportional to $f_{11}f_{22}/M_{\Phi_6}^2$. The off-diagonal coupling f_{ij} will contribute to flavor violation processes, for instance $D \to \pi\pi$ which is proportional to $f_{12}f_{11}/M_{\Phi_6}^2$. The current bounds require that

$$f_{11}f_{22} \lesssim 10^{-6}; f_{11}f_{12} \lesssim 10^{-2}, \qquad (5.3)$$

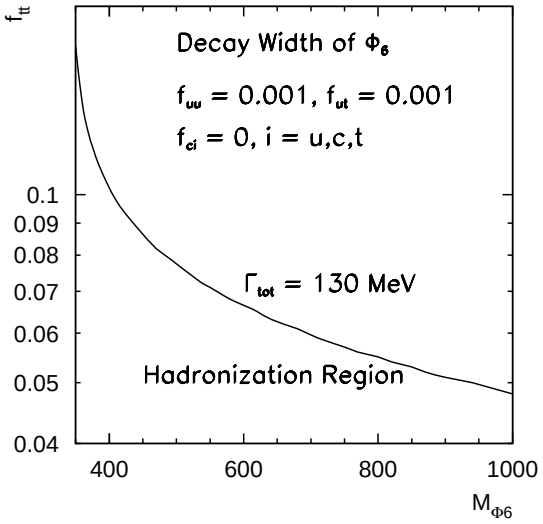

Figure 5.1: Decay-width contour for Φ_6 in the mass and coupling plane.

for M_{Φ_6} of a few hundred GeV to TeV mass range [72, 76, 77]. One will also expect less stringent constraints from a one-loop process such as $c \to u\gamma$. To escape from the bound, for accessible values of M_{Φ_6} we expect at least one of the couplings, f_{11} or f_{22}, to be negligible. However, from our purely phenomenological perspective, we take the decay branching fraction BR$(\Phi_6 \to tt)$ to be a completely free parameter whose value may be determined at the LHC.

Because the sextet is a colored object, we need to consider the possibility of it hadronizing before decaying. For example, it may form a tetraquark-like bound state with $\bar{3}\bar{3}$, such as $\Phi_6\bar{u}\bar{u}$, $\Phi_6\bar{u}\bar{d}$, or $\Phi_6\bar{d}\bar{d}$, with charges $0, 1, and 2$, respectively. If the total width is less than $\Lambda_{\rm QCD} \approx m_\pi$, then the colored object will hadronize before it decays. To determine the constraint imposed by the possibility of hadronization, in Fig. 5.1 we plot the contour for which decay width of Φ_6 is equal to $\Lambda_{\rm QCD}$ as a function of the couplings and the mass. Setting $f_{uu} = 0.001$, $f_{ut} = 0.001$, and eliminating any coupling to c, we see the possibility that a large portion of our parameter space will be protected from the risk of hadronization.

5.2 Production of Φ_6

Because it carries color, Φ_6 can be produced directly through the QCD strong interaction at the LHC. The pair of $\bar{\Phi}_6\Phi_6$ is produced from gluon-gluon fusion or $q\bar{q}$ annihilation:

$$\begin{aligned} g(p_1) + g(p_2) &\to \bar{\Phi}_6(k_1) + \Phi_6(k_2) \\ q(p_1) + \bar{q}(p_2) &\to \bar{\Phi}_6(k_1) + \Phi_6(k_2). \end{aligned} \tag{5.4}$$

The total production cross section depends only on the mass of Φ_6, since the vertex is just the strong coupling, g_s, as shown in Eq. (5.6). By comparison, the electroweak production of $\bar{\Phi}_6\Phi_6$ is small enough to be neglected in our search.

d_R	3	6	8
$C(R)$	1/2	5/2	3
$C_2(R)$	4/3	10/3	3

Table 5.1: Normalization factor $C(R)$ and quadratic Casimir $C_2(R)$ for $d_R = 3, 6, 8$ under $SU(3)$.

From the scalar QCD gauge interaction

$$(D_\mu \Phi_6)^\dagger (D^\mu \Phi_6), \text{ where } D_\mu = \partial_\mu - i g_s G^a_\mu T^a, \tag{5.5}$$

one may obtain the Feynman rules

$$\begin{aligned} G^a_\mu \Phi_6 \bar{\Phi}_6 &: i g_s (p_1 - p_2)_\mu T^a \\ G^a_\mu G^b_\nu \Phi_6 \bar{\Phi}_6 &: -i g_s^2 g_{\mu\nu} (T^a T^b + T^b T^a). \end{aligned} \tag{5.6}$$

The momenta are assigned according to $V_\mu S(p_1) \bar{S}(p_2)$ and all momenta are outgoing. In group-theory langauge, this is $6 \otimes \bar{6} = 27 \oplus 8 \oplus 1$.

The parton-level cross sections for a color sextet pair production are given by

$$\sigma(q\bar{q} \to \bar{\Phi}_6 \Phi_6) = \pi C(3) C(R) \frac{d_8}{d_3^2} \frac{\alpha_s^2}{3s} \beta^3 = \frac{10\pi}{27s} \alpha_s^2 \beta^3 \tag{5.7}$$

and

$$\begin{aligned} \sigma(gg \to \bar{\Phi}_6 \Phi_6) &= d_R C_2(R) \pi \frac{\alpha_s^2}{6s} \frac{1}{d_8^2} [3\beta(3 - 5\beta^2) - 12 C_2(R) \beta(\beta^2 - 2) \\ &+ \ln|\frac{\beta+1}{\beta-1}| (6 C_2(R)(\beta^4 - 1) - 9(\beta^2 - 1)^2] \\ &= \frac{5\pi}{96s} \alpha_s^2 [\beta(89 - 55\beta^2) + \ln|\frac{\beta+1}{\beta-1}| (11\beta^4 + 18\beta^2 - 29)] \,, \end{aligned} \tag{5.8}$$

where $\sqrt{s}$ is the total energy, $\beta = \sqrt{1 - 4M^2_{\Phi_6}/s}$, and R is 6 with the normalization factor C and Casimir C_2 satisfying

$$\text{Tr}[T^a_R T^b_R] = C(R) \delta^{ab} \text{ and } T^a_R T^a_R = C_2(R) \mathbf{1}. \tag{5.9}$$

We list the values for different representations under $SU(3)$ in Table 5.1.

The QCD production cross sections for the color sextet scalar pair $\bar{\Phi}_6 \Phi_6$ at both LHC and Tevatron are plotted in Fig. 5.2 with factorization scale $\mu_F = M_{\Phi_6}$, renormalization scale $\mu_R = m_Z$, and the CTEQ6L [78] parton distribution function (PDF). The matrix elements in our calculations here and elsewhere are generated by SUSY-Madgraph [79] with modified color factors. For comparison, we also show the pair-production cross sections for $SU(3)_C$ triplet and octet scalars at the LHC. As we can see, the total production cross section of the sextet scalar is similar to that of the octet scalar, but is about one order maginitude larger than that of the triplet scalar, which can be understood from values of C and C_2 for different reprensentations in Table 5.1.

As discussed in the introduction, the color sextet scalar Φ_6 only couples to the righthanded up-type quark-quark pair. Thus, we may also have single production of a Φ_6 through

$$uu(cc) \to \Phi_6. \tag{5.10}$$

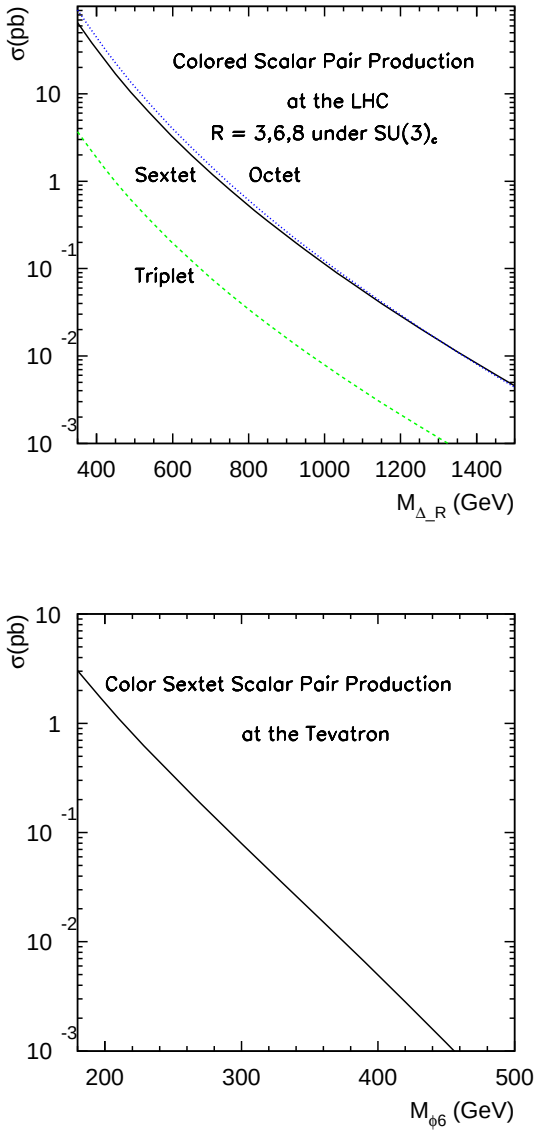

Figure 5.2: Production of $\bar{\Phi}_6\Phi_6$ at the LHC and Tevatron with $\mu_F = M_{\Phi_6}$, fixed scale $\alpha_S(\mu_R)$ with $\mu_R = m_Z$. The PDF set CTEQ6L has been used in all calculations.

However, the production cross section is proportional to the coupling $|f_{uu}|^2$ and $|f_{cc}|^2$, and may therefore be suppressed due to the $D^0 - \bar{D}^0$ mixing constraint. Some studies of the single Φ_6 production at the Tevatron and the LHC have been done in Ref. [72].

5.3 Searching for the Color Sextet Scalar through $tt\overline{tt}$

As discussed in the previous sections, the most distinct feature of the color sextet scalar is its decay mode $\Phi_6 \to tt$, which leads to a same-sign dilepton signature in the final state if both top quarks decay semileptonically, i.e., $t \to W^+b \to \ell^+\nu b$. To avoid ambiguities in lepton assignments during reconstruction, we require the anti-top quark pair from the $\bar{\Phi}_6$ to decay hadronically. Hence, the final state of $\bar{\Phi}_6\Phi_6$ is

$$pp \to \bar{\Phi}_6\Phi_6 \to tt\overline{tt} \to 4b + \ell^\pm\ell^\pm + \not{E}_T + Nj, \tag{5.11}$$

where $\ell = e$ and μ, and $N \geq 4$ to allow initial and final state QCD radiation. In our study, however, the QCD radiation is not included. To get this final state, the decay branching ratio will be

$$\text{BR} = \text{BR}^2(\Phi_6 \to tt) \times \left(\frac{2}{9}\right)^2 \times \left(\frac{2}{3}\right)^2 \times 2, \tag{5.12}$$

where the situation that the top quark decays hadronically and the anti-top quark decays semileptonically is also included. Figure 5.2 also clearly shows that a color sextet with $M_{\Phi_6} \geq 350$ GeV will not be bounded by Tevatron data as the same-sign dilepton plus multi-jet final state from $tt\bar{t}\bar{t}$ will be less than one event for 2 fb^{-1} luminosity.

To illustrate the kinematic features of the color sextet scalar pair, we consider the decay process $\Phi_6\bar{\Phi}_6 \to tt\overline{tt} \to bb\bar{b}\bar{b}\ell^+\ell^{'+} + 4$ jets and take $M_{\Phi_6} = 600$ GeV. The leading and second-leading jet p_T distributions are shown in Fig. 5.3. The typical hardness of these jets is the basis for one of our selection cuts introduced later in this section. In order simulate the detector effects on the energy-momentum measurements, we smear the electromagnetic energy and the muon momentum by a Gaussian distribution whose width is parameterized as [80]

$$\frac{\Delta E}{E} = \frac{a_{cal}}{\sqrt{E/\text{GeV}}} \oplus b_{cal}, \quad a_{cal} = 5\%, b_{cal} = 0.55\%, \tag{5.13}$$

$$\frac{\Delta p_T}{p_T} = \frac{a_{track}p_T}{\text{TeV}} \oplus \frac{b_{track}}{\sqrt{\sin\theta}}, \quad a_{track} = 15\%, b_{track} = 0.5\%. \tag{5.14}$$

The jet energies are also smeared using the same Gaussian formula as in Eq. (5.13), but with [80]

$$a_{cal} = 100\%, \quad b_{cal} = 5\%. \tag{5.15}$$

We first reconstruct the two on-shell hadronically decaying W's. Our procedure is to consider all dijet invariant masses except for those containing one of the two tagged b-jets, since we require b-tagging in the event selection discussed later, and choose the two closest M_{jj} combinations, which we then require to lie within the mass window

$$|M_{jj} - m_W| < 15\text{GeV}. \tag{5.16}$$

From this, we get the two reconstructed W momenta. We then consider all combinations of reconstructed p_W with all jets and again choose the two closest invariant masses M_{jW}. In this way, we reconstruct the two hadronically decaying anti-top quarks. The distributions of these reconstructed invariant masses are shown in Fig. 5.4.

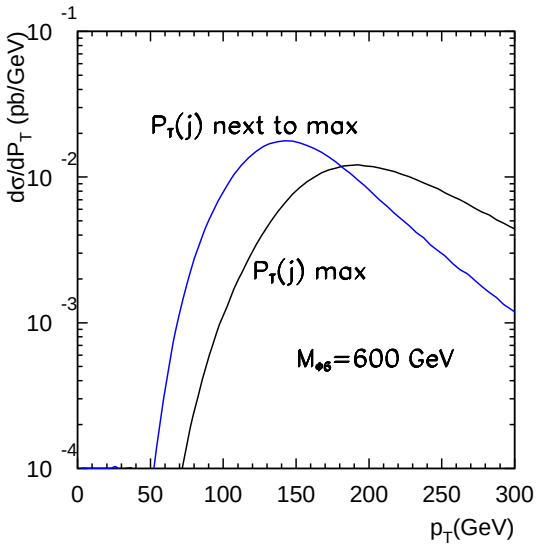

Figure 5.3: max$\{p_T^J\}$ and next-to-max$\{p_T^J\}$

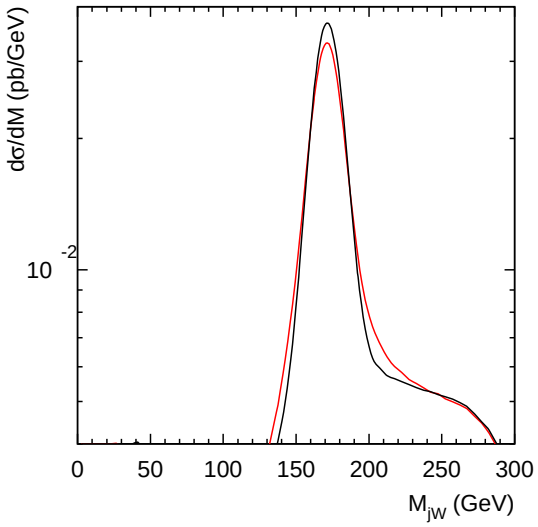

Figure 5.4: Reconstructed hadronic top pair. The black(red) line represents the first(second) reconstructed hadronically decaying anti-top quark.

Once we have the reconstructed two anti-top quarks, the reconstruction of the sextet $(\bar{\Phi})$ can be done using the 6-jet invariant mass M_{6j} for the two hadronic anti-top quarks. Although the production of neutrinos prevents us from fully reconstructing the sextet which produces the leptonic decays, we may

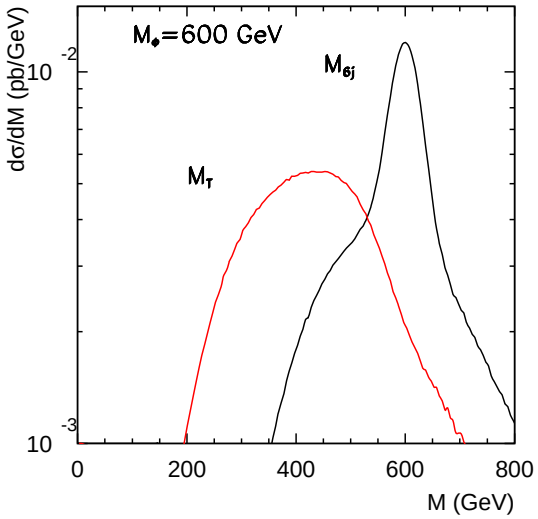

Figure 5.5: Reconstructed Sextet from m_{6j} and M_T.

reconstruct the transverse mass M_T for the remaining two jets plus same-sign dilepton and $\not{E}_T$ as

$$M_T = \sqrt{(\sum_j E_T + \sum_\ell E_T + \not{E}_T)^2 - (\sum \vec{p}(j) + \sum \vec{p}(\ell) + \not{p})^2_T}. \tag{5.17}$$

As seen in Fig. 5.5, our reconstruction shows a clear resonance in both the M_{6j} and M_T distributions.

Finally, since the two anti-top quarks may be fully reconstructed, we can boost back to the rest frame of the $\bar{\Phi}_6$ and study its spin. As shown in Fig. 5.6, the angular distribution of the anti-quark clearly shows that the $\bar{\Phi}_6$ is a scalar. Since there are two missing neutrinos from the decay of two top quarks, it is challenging to fully reconstruct the top quark's momentum, and study the spin information of top quarks, which can be used to check this model since Φ_6 only decays into a right-handed top quark pair. We leave this for future work.

We next consider the backgrounds for our signal. We require at least 2 tagged b-jets plus a same-sign dilepton and multijet. The irreducible SM background for this final state consists of $t\bar{t}W^\pm + Nj$, $bb + W^\pm W^\pm + Nj$ and $t\bar{t}t\bar{t}$. We estimate the QCD $bb + W^\pm W^\pm + Nj$ background by computing $jjW^\pm W^\pm$ production. This is only 14 fb, and one expects that the $bb + W^\pm W^\pm + Nj$ is about three orders of magnitude lower and therefore $\lesssim 0.1$ fb. The SM 4-top $t\bar{t}t\bar{t}$ is less than 0.1 fb to start with. The leading background thus comes from $t\bar{t}W^\pm$ with one hadronic top decay and one semileptonic top decay with the same sign as $W^\pm$ leptonic decay.

We propose the following selection cuts:

- min$\{p_T(j)\} > 15$ GeV, max$\{p_T(j)\} > 100$ GeV, next-to-max$\{p_T(j)\} > 75$ GeV, $|\eta(j) < 3.0|$;
- same-sign dilepton with $p_T(\ell) > 15$ GeV, $|\eta(\ell) < 2.8|$;
- $\Delta R_{jj},\ \Delta R_{jl},\ \Delta R_{ll} > 0.4$;

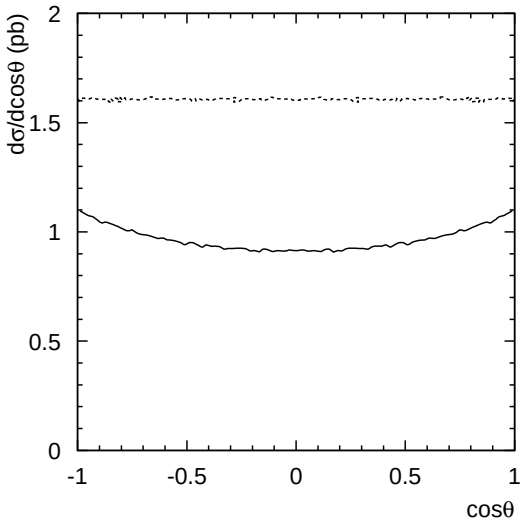

Figure 5.6: Distribution of $\cos\theta$ between reconstructed top momentum and reconstructed sextet momentum. Dashed(solid) line shows the distribution without(with) smearing effects and kinematic cuts.

- at least two b-tagged jets; and
- $\not{E}_T > 25$ GeV.

Since the production rate of our signal only depends on the mass M_{Φ_6} and the branching ratio of Φ_6 decay to a top-quark pair, we scan these two parameters to study the discovery potential. We summarize our results in Fig. 5.7 as the signal production rate for $bb\bar{b}\bar{b} + \ell^\pm\ell^\pm + \not{E}_T + 4j$ from $\Phi_6\bar{\Phi}_6$ with SM $t\bar{t}W^\pm$ background included. We use a factor of 25% in both plots in Fig. 5.7 for tagging two b jets with 50% effeciency to tag each b-jet. The SM background is taken as 1 fb in the significance contour. As we can see in the left plot of Fig. 5.7, for 100 fb^{-1} luminosity, the statistical significance can surpass the 5σ level for $M_{\Phi_6} \lesssim 800\text{GeV}$ if BR($\Phi \to tt$) is about 0.5. Also note that the mass of the sextet scalar can be determined by reconstructing two hadronically decaying top (or anti-top) quarks, and the branching ratio of $\Phi_6 \to tt$ can be roughly estimated from the total signal event rate if one can understand the background sufficiently well. No reconstruction selection has been implemented since we did not simulate the events with initial state/final state radiation and the reconstruction efficiency is thus unknown. In principle, we expect that the $S/\sqrt{B}$ can be further improved by including reconstruction.

5.4 Conclusion

In this chapter, we discuss the production of a new exotic particle, a color sextet scalar, at the CERN Large Hadron Collider. Taking a purely phemenological approach, we discuss the discovery of the color sextet scalar through its decay into a top-top quark pair. The unique feature of same-sign dilepton plus multijet makes it easy to identify and reconstruct the color sextet scalar object. Due to its

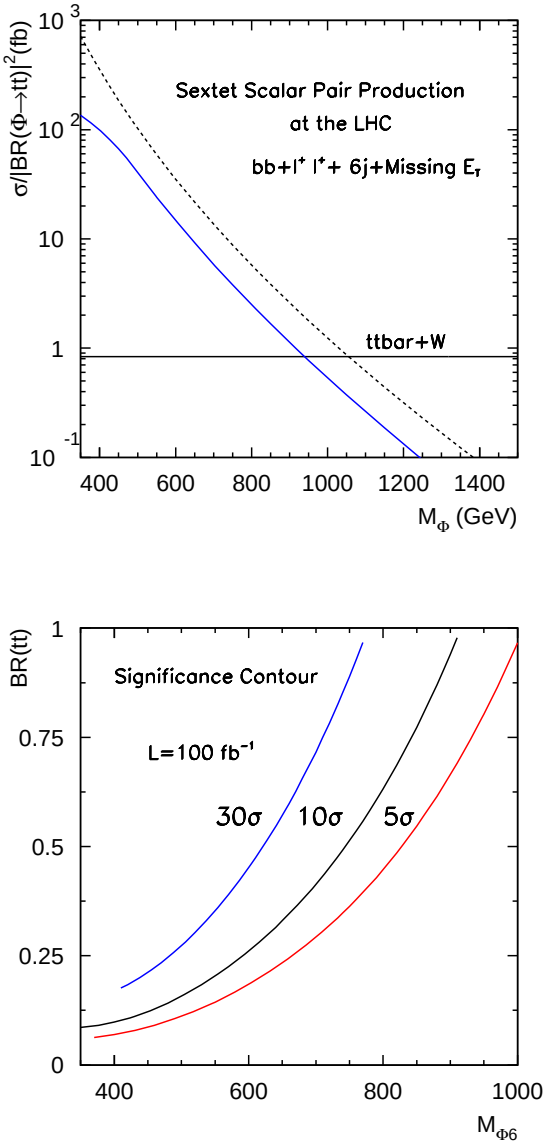

Figure 5.7: Production rate normalized by BR$(\Phi_6 \to tt)^2$ and significance contour. Dashed(solid) curves in the left plot represent production before(after) selection cuts.

large QCD production, it is possible to cover the color sextet scalar up to a mass range of 1 TeV for 100 fb^{-1} integrated luminosity.

In the text, we only consider the case of $M_{\Phi_6} > 2m_t$, where Φ_6 decays into two on-shell top quarks. In the case $2M_{\Phi_6} < m_Z$, there is a possiblity of a Z decaying into a sextet pair, since Φ_6 carries a $U(1)_Y$ charge, which we expect is highly constrained by LEP data. We also expect to find strong constraints from Tevatron data. For example, for M_{Φ_6} just above $m_t + m_b$ threshold, the $\bar{\Phi}_6\Phi_6$ signal

will directly contribute to the $t\bar{t}X$ sample as the off-shell top decay products are soft.

Chapter 6

Conclusions

The coming years should be an exciting time in particle physics. With the LHC already up and running at 7 TeV center-of-mass energy and further expected luminosity and beam-energy upgrades, we expect to finally probe the electroweak scale. Besides finding the Higgs boson, we expect to discover a wealth of new particles. Measuring the spins of these new particles will be crucial in determining the correct underlying theory of BSM physics. We expect that with about 100-500 $\text{fb}^{-}1$ of integrated luminosity, we will be able to measure spins with good accuracy in cases where there is no missing energy. However, most new physics scenarios predict signals with missing energy, and they pose a serious problem, hampering reconstruction and hence spin determination. New reconstruction schemes which do not sacrifice too much on statistics will likely be needed if we are to probe spins of new particles in a model-independent way in the most favored scenarios such as SUSY and UED. In the future, the ILC may be able to probe these scenarios more accurately.

In addition, it should be remembered that the LHC is really the most powerful QCD machine ever built. It is an ideal testing ground for theories of new strongly interacting particles such as color sextets. The striking "same-sign dilepton" signature of color sextet decay makes it one of the easiest exotic particles to observe at the LHC.

Bibliography

[1] M. R. Buckley, H. Murayama, W. Klemm and V. Rentala, Phys. Rev. D **78**, 014028 (2008) [arXiv:0711.0364 [hep-ph]].

[2] H. Murayama and V. Rentala, arXiv:0904.4561 [hep-ph].

[3] C. R. Chen, W. Klemm, V. Rentala and K. Wang, Phys. Rev. D **79**, 054002 (2009) [arXiv:0811.2105 [hep-ph]].

[4] S. P. Martin, arXiv:hep-ph/9709356.

[5] C. Csaki, arXiv:hep-ph/0404096.

[6] S. Weinberg, Phys. Rev. D **13**, 974 (1976).

[7] S. Weinberg, Phys. Rev. D **19**, 1277 (1979).

[8] L. Susskind, Phys. Rev. D **20**, 2619 (1979).

[9] G. t Hooft, in *Recent developments in gauge theories,* Proceedings of the NATO Advanced Summer Institute, Cargese 1979, ed. G. t Hooft *et al.* (Plenum, New York 1980).

[10] J. Wess and B. Zumino, Nucl. Phys. B **70**, 39 (1974).

[11] N. Arkani-Hamed, S. Dimopoulos and G. R. Dvali, Phys. Lett. B **429**, 263 (1998) [arXiv:hep-ph/9803315].

[12] N. Arkani-Hamed, S. Dimopoulos and G. R. Dvali, Phys. Rev. D **59**, 086004 (1999) [arXiv:hep-ph/9807344].

[13] I. Antoniadis, N. Arkani-Hamed, S. Dimopoulos and G. R. Dvali, Phys. Lett. B **436**, 257 (1998) [arXiv:hep-ph/9804398].

[14] I. Antoniadis, Phys. Lett. B **246**, 377 (1990).

[15] I. Antoniadis and K. Benakli, Phys. Lett. B **326**, 69 (1994) [arXiv:hep-th/9310151].

[16] L. Randall and R. Sundrum, Phys. Rev. Lett. **83**, 3370 (1999) [arXiv:hep-ph/9905221].

[17] L. Randall and R. Sundrum, Phys. Rev. Lett. **83**, 4690 (1999) [arXiv:hep-th/9906064].

[18] M. Weinstein, Phys. Rev. D **8**, 2511 (1973).

[19] N. Arkani-Hamed, A. G. Cohen and H. Georgi, Phys. Lett. B **513**, 232 (2001) [arXiv:hep-ph/0105239].

[20] T. Appelquist, H. C. Cheng and B. A. Dobrescu, Phys. Rev. D **64**, 035002 (2001) [arXiv:hep-ph/0012100].

[21] H. C. Cheng, K. T. Matchev and M. Schmaltz, Phys. Rev. D **66**, 056006 (2002) [arXiv:hep-ph/0205314].

[22] K. Kong and K. T. Matchev, AIP Conf. Proc. **903**, 451 (2007) [arXiv:hep-ph/0610057].

[23] M. Battaglia, A. K. Datta, A. De Roeck, K. Kong and K. T. Matchev, *In the Proceedings of 2005 International Linear Collider Workshop (LCWS 2005), Stanford, California, 18-22 Mar 2005, pp 0302* [arXiv:hep-ph/0507284].

[24] G. Burdman, B. A. Dobrescu and E. Ponton, Phys. Rev. D **74**, 075008 (2006) [arXiv:hep-ph/0601186].

[25] M. Battaglia, A. Datta, A. De Roeck, K. Kong and K. T. Matchev, JHEP **0507**, 033 (2005) [arXiv:hep-ph/0502041].

[26] S. Y. Choi, K. Hagiwara, H. U. Martyn, K. Mawatari and P. M. Zerwas, Eur. Phys. J. C **51**, 753 (2007) [arXiv:hep-ph/0612301].

[27] L. T. Wang and I. Yavin, JHEP **0704**, 032 (2007) [arXiv:hep-ph/0605296].

[28] A. J. Barr, Phys. Lett. B **596**, 205 (2004) [arXiv:hep-ph/0405052].

[29] A. J. Barr, JHEP **0602**, 042 (2006) [arXiv:hep-ph/0511115].

[30] J. M. Smillie and B. R. Webber, JHEP **0510**, 069 (2005) [arXiv:hep-ph/0507170].

[31] A. Alves and O. Eboli, Phys. Rev. D **75**, 115013 (2007) [arXiv:0704.0254 [hep-ph]].

[32] H. Murayama, International Linear Collider Workshop (LCWS2000), Oct. 24-28, 2000, Fermilab

[33] R. Schwitters *et al.*, Phys. Rev. Lett. **35**, 1320 (1975).

[34] H. Murayama, I. Watanabe and K. Hagiwara, "HELAS: HELicity Amplitude Subroutines for Feynman diagram evaluations."

[35] S. Kawabata, "A New Monte Carlo Event Generator For High-Energy Physics," Comput. Phys. Commun. **41**, 127 (1986).

[36] D. Berdine, N. Kauer and D. Rainwater, Phys. Rev. Lett. **99**, 111601 (2007) [arXiv:hep-ph/0703058].

[37] T. Tsukamoto, K. Fujii, H. Murayama, M. Yamaguchi and Y. Okada, Phys. Rev. D **51**, 3153 (1995).

[38] H. C. Cheng, J. F. Gunion, Z. Han, G. Marandella and B. McElrath, arXiv:0707.0030 [hep-ph].

[39] P. B. Wilson, "Future e+e- Linear colliders and beam-beam effects," SLAC-PUB-3985, May 1986.

[40] A. Freitas *et al.*, arXiv:hep-ph/0211108.

[41] J. L. Feng and M. E. Peskin, Phys. Rev. D **64**, 115002 (2001) [arXiv:hep-ph/0105100].

[42] T. Behnke, S. Bertolucci, R. D. Heuer and R. Settles, "TESLA: The superconducting electron positron linear collider with an integrated X-ray laser laboratory. Technical design report. Pt. 4: A detector for TESLA," `http://tesla.desy.de/new_pages/TDR_CD/start.html`

[43] H. Murayama and M. E. Peskin, Ann. Rev. Nucl. Part. Sci. **46**, 533 (1996) [arXiv:hep-ex/9606003].

[44] N. Ghodbane and H. U. Martyn, in *Proc. of the APS/DPF/DPB Summer Study on the Future of Particle Physics (Snowmass 2001)* ed. N. Graf, arXiv:hep-ph/0201233.

[45] B. C. Allanach *et al.*, in *Proc. of the APS/DPF/DPB Summer Study on the Future of Particle Physics (Snowmass 2001)* ed. N. Graf, *In the Proceedings of APS / DPF / DPB Summer Study on the Future of Particle Physics (Snowmass 2001), Snowmass, Colorado, 30 Jun - 21 Jul 2001, pp P125* [arXiv:hep-ph/0202233].

[46] H. C. Cheng, K. T. Matchev and M. Schmaltz, Phys. Rev. D **66**, 036005 (2002) [arXiv:hep-ph/0204342].

[47] `http://home.fnal.gov/~kckong/mued/`

[48] A. Pukhov, arXiv:hep-ph/0412191.

[49] F. E. Paige, arXiv:hep-ph/9801254.

[50] C. Csaki and Y. Shirman, [arXiv:hep-th/9908186]; J. Lykken and L. Randall, [arXiv:hep-th/9908076]; I. Oda, [arXiv:hep-th/9908104,hep-th/9909048]; T. Li, [arXiv:hep-th/9911234]; N. Arkani-Hamed, S. Dimopoulos, G. Dvali and N. Kaloper, [arXiv:hep-th/9907209]; I.I. Kogan *et al*, [arXiv:hep-ph/9912552]

[51] H. Davoudiasl, J. L. Hewett and T. G. Rizzo, Phys. Rev. Lett. **84**, 2080 (2000) [arXiv:hep-ph/9909255].

[52] H. Davoudiasl, J. L. Hewett and T. G. Rizzo, Phys. Rev. D **63**, 075004 (2001) [arXiv:hep-ph/0006041].

[53] B. C. Allanach, K. Odagiri, M. A. Parker and B. R. Webber, JHEP **0009**, 019 (2000) [arXiv:hep-ph/0006114].

[54] P. Osland, A. A. Pankov, N. Paver and A. V. Tsytrinov, Phys. Rev. D **78**, 035008 (2008) [arXiv:0805.2734 [hep-ph]].

[55] P. Osland, A. A. Pankov, A. V. Tsytrinov and N. Paver, arXiv:0902.1593 [hep-ph].

[56] M. R. Buckley, B. Heinemann, W. Klemm and H. Murayama, Phys. Rev. D **77**, 113017 (2008) [arXiv:0804.0476 [hep-ph]].

[57] G. F. Giudice, R. Rattazzi and J. D. Wells, Nucl. Phys. B **544**, 3 (1999) [arXiv:hep-ph/9811291].

[58] T. Han, J. D. Lykken and R. J. Zhang, Phys. Rev. D **59**, 105006 (1999) [arXiv:hep-ph/9811350].

[59] K. Agashe, H. Davoudiasl, G. Perez and A. Soni, Phys. Rev. D **76**, 036006 (2007) [arXiv:hep-ph/0701186].

[60] I. Belotelov *et al.*, CERN-CMS-NOTE-2006-104

[61] P. Traczyk and G. Wrochna, arXiv:hep-ex/0207061.

[62] V. M. Abazov *et al.* [D0 Collaboration], Phys. Rev. Lett. **95**, 091801 (2005) [arXiv:hep-ex/0505018].

[63] "ATLAS: Detector and physics performance. Technical design report. Volume 1,"

[64] "ATLAS detector and physics performance. Technical design report. Vol. 2,"

[65] K. Hagiwara, J. Kanzaki, Q. Li and K. Mawatari, Eur. Phys. J. C **56**, 435 (2008) [arXiv:0805.2554 [hep-ph]].

[66] M. R. Whalley, D. Bourilkov and R. C. Group, arXiv:hep-ph/0508110.

[67] J. Pumplin, D. R. Stump, J. Huston, H. L. Lai, P. M. Nadolsky and W. K. Tung, JHEP **0207**, 012 (2002) [arXiv:hep-ph/0201195].

[68] S. Errede and S. H. H. Tye, Summary Report of the Stable/Exotic Particles Working Group on SSC, Snowmass, 1984. H. Tanaka and I. Watanabe, Int. J. Mod. Phys. A **7**, 2679 (1992).

[69] J. C. Pati and A. Salam, Phys. Rev. D **10**, 275 (1974) [Erratum-ibid. D **11**, 703 (1975)]. R. N. Mohapatra and R. E. Marshak, Phys. Rev. Lett. **44**, 1316 (1980) [Erratum-ibid. **44**, 1643 (1980)].

[70] P. Fileviez Perez, Phys. Lett. B **654**, 189 (2007) [arXiv:hep-ph/0702287].

[71] Z. Chacko and R. N. Mohapatra, Phys. Rev. D **59**, 055004 (1999) [arXiv:hep-ph/9802388].

[72] R. N. Mohapatra, N. Okada and H. B. Yu, Phys. Rev. D **77**, 011701 (2008) [arXiv:0709.1486 [hep-ph]].

[73] See for example: V. Barger, T. Han and D. G. E. Walker, Phys. Rev. Lett. **100**, 031801 (2008) [arXiv:hep-ph/0612016]. B. Lillie, L. Randall and L. T. Wang, JHEP **0709**, 074 (2007) [arXiv:hep-ph/0701166]. A. L. Fitzpatrick, J. Kaplan, L. Randall and L. T. Wang, JHEP **0709**, 013 (2007) [arXiv:hep-ph/0701150]. B. Lillie, J. Shu and T. M. P. Tait, JHEP **0804**, 087 (2008) [arXiv:0712.3057 [hep-ph]]. T. Han, arXiv:0804.3178 [hep-ph]. Y. Bai and Z. Han, arXiv:0809.4487 [hep-ph]. T. Plehn and T. M. P. Tait, arXiv:0810.3919 [hep-ph].

[74] K. S. Babu, R. N. Mohapatra and S. Nasri, Phys. Rev. Lett. **97**, 131301 (2006) [arXiv:hep-ph/0606144].

[75] L. J. Hall and A. E. Nelson, Phys. Lett. B **153**, 430 (1985). R. S. Chivukula, M. Golden and E. H. Simmons, Nucl. Phys. B **363**, 83 (1991). M. I. Gresham and M. B. Wise, Phys. Rev. D **76**, 075003 (2007) [arXiv:0706.0909 [hep-ph]]. B. A. Dobrescu, K. Kong and R. Mahbubani,

arXiv:0709.2378 [hep-ph]. M. Gerbush, T. J. Khoo, D. J. Phalen, A. Pierce and D. Tucker-Smith, Phys. Rev. D **77**, 095003 (2008) [arXiv:0710.3133 [hep-ph]].

C. Kilic, T. Okui and R. Sundrum, JHEP **0807**, 038 (2008) [arXiv:0802.2568 [hep-ph]]. M. V. Martynov and A. D. Smirnov, arXiv:0807.4486 [hep-ph]. P. Fileviez Perez, R. Gavin, T. McElmurry and F. Petriello, arXiv:0809.2106 [hep-ph]. C. Kilic, S. Schumann and M. Son, arXiv:0810.5542 [hep-ph].

[76] M. Staric *et al.* [Belle Collaboration], Phys. Rev. Lett. **98**, 211803 (2007) [arXiv:hep-ex/0703036].

[77] C. Amsler *et al.* [Particle Data Group], Phys. Lett. B **667**, 1 (2008).

[78] J. Pumplin, D. R. Stump, J. Huston, H. L. Lai, P. M. Nadolsky and W. K. Tung, JHEP **0207**, 012 (2002) [arXiv:hep-ph/0201195].

[79] G. C. Cho, K. Hagiwara, J. Kanzaki, T. Plehn, D. Rainwater and T. Stelzer, Phys. Rev. D **73**, 054002 (2006) [arXiv:hep-ph/0601063].

[80] CMS TDR: CMS Physics: Technical Design Report V.2: Physics Performance, CERN-LHCC-2006-021. ATLAS TDR: ATLAS detector and physics performance. Technical design report. Vol. 2, CERN-LHCC-99-15